Molecular Clouds in the Milky Way

Mark Heyer[1] and T.M. Dame[2]

[1]Department of Astronomy, University of Massachusetts, Amherst, Massachusetts 01003; email: heyer@astro.umass.edu

[2]Harvard-Smithsonian Center for Astrophysics, Cambridge, Massachusetts 02138; email: tdame@cfa.harvard.edu

Annu. Rev. Astron. Astrophys. 2015. 53:583–629

The *Annual Review of Astronomy and Astrophysics* is online at astro.annualreviews.org

This article's doi:
10.1146/annurev-astro-082214-122324

Keywords

Galaxy: disk, structure; ISM: clouds, kinematics and dynamics, molecules; radio lines: ISM

Abstract

In the past twenty years, the reconnaissance of ^{12}CO and ^{13}CO emission in the Milky Way by single-dish millimeter-wave telescopes has expanded our view and understanding of interstellar molecular gas. We enumerate the major surveys of CO emission along the Galactic plane and summarize the various approaches that leverage these data to determine the large-scale distribution of molecular gas: its radial and vertical distributions, its concentration into clouds, and its relationship to spiral structure. The integrated properties of molecular clouds are compiled from catalogs derived from the CO surveys using uniform assumptions regarding the Galactic rotation curve, solar radius, and the CO-to-H_2 conversion factor. We discuss the radial variations of cloud surface brightness, the distributions of cloud mass and size, and scaling relations between velocity dispersion, cloud size, and surface density that affirm that the larger clouds are gravitationally bound. Measures of density structure and gas kinematics within nearby, well-resolved clouds are examined and attributed to the effects of magnetohydrodynamic turbulence. We review the arguments for short, intermediate, and long molecular lifetimes based on the observational record. The review concludes with questions that shall require further observational attention.

1. INTRODUCTION

I've looked at clouds from both sides now/From up and down, and still somehow
It's cloud illusions I recall/I really don't know clouds at all —Joni Mitchell

The detections of interstellar molecular hydrogen (H_2) in the UV (Carruthers 1970) and carbon monoxide (CO) at 2.6 mm (Wilson et al. 1970) spawned an exciting new era of research on the molecular interstellar medium (ISM). Although the presence of molecules in space had been recognized as early as 1937 from optical absorption studies (Swings & Rosenfeld 1937) and further revealed in the 1960s using microwave techniques to detect OH (Weinreb et al. 1963), NH_3 (Cheung et al. 1968), water (Cheung et al. 1969), and formaldehyde (Snyder et al. 1969), the direct measure of the dominant constituent, H_2, validated, in part, theoretical predictions (Gould & Salpeter 1963, Solomon & Wickramasinghe 1969, Hollenbach et al. 1971) and accounted for excess extinction measured in local clouds (Heiles 1969). Large reservoirs of H_2 gas were predicted in high column density ($>10^{21}$ cm^{-2}) regions where dust extinction precludes the use of UV spectroscopy. The $J = 1$–0 rotational transition of CO at a frequency of 115 GHz and line emission from other molecules in the millimeter band offered an accessible and valuable spectroscopic proxy to molecular hydrogen in this high column density regime. Once the link between star formation and molecular gas was established, both theoretical and observational efforts accelerated.

In the subsequent four decades, millimeter and submillimeter facilities have been constructed to investigate the molecular ISM through spectroscopy and the thermal continuum emission from dust grains. These millimeter and submillimeter observations are complemented by X-ray, UV/optical/IR, far-IR, and radio (centimeter wave) measurements and evolving theoretical descriptions of the complex physics of these regions. This strong interest in the molecular ISM and star formation continues to this day with the scientific operations of the Atacama Large Millimeter Array, a major international facility that explores the molecular ISM of distant and local galaxies, molecular star-forming regions in the Milky Way, and the molecular, circumstellar disks and planetary systems of newborn stars.

In this contribution, we review the distribution and physics of the molecular ISM in the Milky Way; our conclusions are primarily derived from observations of the lowest rotational transition of CO and its isotopologue, ^{13}CO, collected over the past 20 years since the review by Combes (1991) in this series. There are compelling reasons to investigate the molecular gas content of our own Galaxy. Observations of interstellar features and processes in the Milky Way offer the highest spatial resolution possible, enabling detailed physical descriptions and tests of theory. Although our Galaxy is just one of billions in the Universe, the compilation of properties in the Milky Way is the fundamental basis to gauge similar attributes derived from measurements of other galaxies. Any similarities or differences are valuable clues to the processes that affect the molecular gas content and the production of newborn stars. Finally, the Milky Way is the galaxy in which we reside. Establishing the stellar and gas structure of the Milky Way and the Sun's relationship to that structure provides an awareness of our cosmic neighborhood and our journey through the Galaxy.

Such a review is timely given the improved quality of current data compared with that available 20 years ago and the development of more sophisticated analysis methods to exploit this added information. The high-quality data are a result of perseverance to fully sample molecular gas tracers over the entire disk and high-latitude regions of the Milky Way; improved detector sensitivities; and the deployment of millimeter, heterodyne focal plane arrays on moderate-sized (14-m) to large (30–45-m) telescopes that allow high spatial dynamic range imaging of the Galactic plane

and targeted molecular regions (Erickson et al. 1999, Sunada et al. 2000, Schuster et al. 2004, Smith et al. 2008).

Although there are advantages to investigating the ISM of our own Galaxy, there are also significant challenges. Many critical properties of molecular clouds, such as mass and size, depend on their distances. Depending on the applied method, the fractional distance errors can be very large. From our perspective within the Galaxy, it is difficult to establish absolute, spatial relationships of CO emission with other structural features, such as spiral arms or the stellar bar. One can separate molecular features along the line of sight with velocity information, but transforming velocity to position using a rotation curve relies on the assumption of purely circular velocities that is surely invalid for a dissipative medium responding to spatially varying potentials and expansion fronts from supernova remnants, stellar winds, and HII regions. Finally, the internal turbulent motions of molecular regions and Galactic rotation conspire to blend in velocity emission from unrelated structures. This velocity crowding makes it difficult to both identify individual clouds and evaluate the completeness of cloud catalogs (Liszt & Burton 1981, Combes 1991). Some of these observational challenges are removed when examining CO emission from low-inclination galaxies but at the expense of greatly reduced spatial resolution. Thus, a broad understanding of the molecular ISM relies on investigations of both the Milky Way, in which the spatial resolution is optimum, and galaxies that have favorable viewing angles.

There have been several recent reviews in the *Annual Reviews of Astronomy and Astrophysics* and elsewhere that discuss the molecular ISM in relation to star formation (McKee & Ostriker 2007, Hennebelle & Falgarone 2012, Kennicutt & Evans 2012, Krumholz 2014); interstellar turbulence (Scalo & Elmegreen 2004, Elmegreen & Scalo 2004); cold, dark clouds (Bergin & Tafalla 2007); nearby galaxies (Fukui & Kawamura 2010); magnetic fields (Crutcher 2012); and the CO-to-H_2 conversion factor (Bolatto et al. 2013). We have attempted to avoid significant overlap with these summaries while focusing upon results derived from CO observations made with filled aperture telescopes. To structure this review, we pose and address the following questions:

- Are discrete units of CO emission or extinction, i.e., clouds, a valid and useful description of the cold, dense, molecular phase of the ISM?
- What is the H_2 mass of the Milky Way? How is the molecular gas distributed with increasing radius and height above the plane and with respect to spiral structure?
- What are the general properties of molecular clouds as derived from Galactic plane surveys of ^{12}CO and ^{13}CO emission? Do these properties vary with location in the Galaxy in response to changing environment?
- How are molecular clouds structured in mass and velocity?
- What is the evolutionary sequence of molecular clouds as discerned from observations, and what are their typical lifetimes?

2. THE RELATIONSHIP BETWEEN MOLECULAR HYDROGEN AND CARBON MONOXIDE

> We have detected intense line radiation from the direction of the Orion Nebula at a frequency of 115,267.2 MHz. . . . —Wilson et al. (1970)

The large spacing of the rotational levels of the light hydrogen molecule causes it to radiate inefficiently from the dominant fraction of the ISM, which has temperatures below ~200 K. To study this cold, dense molecular phase, astronomers rely on observational surrogates to measure the column density and kinematics of H_2 gas. These measures include extinction and thermal continuum emission from interstellar dust grains, gamma rays produced by cosmic rays

interacting with hydrogen nuclei, and molecular line spectroscopy, most notably, the rotational lines of ^{12}CO and its isotopologues, ^{13}CO and C^{18}O.

CO is the most widely used tracer of H_2 as it offers many advantages over other gas tracers when investigating the molecular ISM in galaxies (Bolatto et al. 2013). Its low rotational transitions ($J_u \leq 4$) occur within the millimeter and submillimeter bands, which are accessible using ground-based telescopes. These transitions lie only 5–22 K above the ground state, enabling CO to probe the coldest regions in the ISM. The critical density for a given molecular transition between upper, u, and lower, l, states is the density at which the rate of spontaneous radiative de-excitation is equal to the collisional de-excitation rate, $n_{crit} = A_{ul}/ <\sigma_{ul} v>$, where A_{ul} is the Einstein A coefficient for the transition and $<\sigma_{ul} v>$ is the collisional rate coefficient averaged over a Maxwellian distribution. For densities several times larger than n_{crit}, the upper state is sufficiently populated by collisions such that the excitation temperature approaches the gas kinetic temperature. CO has a low electric dipole moment (0.1 Debye) and a correspondingly small Einstein A coefficient, which yields a relatively low critical density ($\sim$2,000 cm^{-3} for the $J = 1$–0 transition). For solar metallicity and moderate radiation fields, most of the available interstellar C atoms in the gas phase (those not locked into dust grains) combine with oxygen to form CO in regions with visual extinctions greater than 1–3 magnitudes. The high abundance of ^{12}CO assures that the $J = 1$–0 transition is optically thick in this column density regime. As a result of this high opacity, emitted photons do not readily escape the regions but rather are absorbed to radiatively excite nearby CO molecules. This radiative trapping maintains the excitation of the $J = 1$ level in regions with densities well below the critical density. The combination of high optical depth and thermalized transitions leads to bright lines that can be readily detected and imaged over large areas of the sky. Observations of ^{12}CO emission are complemented by measurements of the low-J transitions of ^{13}CO, which is less abundant by factors of 25–100 in the Milky Way, so its emission has low to moderate optical depths. ^{13}CO $J = 1$–0 emission is well correlated with dust extinction in nearby clouds, providing an indirect link to H_2 column densities (Dickman 1978, Frerking et al. 1982, Lada et al. 1994, J.E. Pineda et al. 2008, J.L. Pineda et al. 2010, Ripple et al. 2013). The ^{13}CO $J = 1$–0 line is sufficiently bright to allow mapping of its distribution over large angular scales along the Galactic plane and in nearby star-forming regions (Bally et al. 1987, Yonekura et al. 1997, Lee et al. 2001, Jackson et al. 2006, Ridge et al. 2006, Narayanan et al. 2008).

The degree to which H_2 and CO molecules are coextensive in the ISM is set by their respective formation and destruction processes and the conditions under which significant abundances of these molecules are sustained. Molecular hydrogen forms primarily on the surfaces of dust grains (Gould & Salpeter 1963, Hollenbach & Salpeter 1971) and is dissociated by a two-step process in which incident UV photons excite the molecule from its electric-vibrational-rotational ground state into the Lyman ($\lambda < 1108$ Å) or Werner ($\lambda < 1008$ Å) bands. For $\sim$15% of these excitations, this step is subsequently followed by radiative de-excitation into an unbound, high-vibrational level within the electronic ground state that dissociates the molecule. The penetration of dissociating UV photons into a hydrogen gas layer is limited by dust attenuation and the line opacity provided by the outer layer of H_2 that self-shields molecules located at larger layer depths. As the opacity increases with increasing depth into the layer, a larger fraction of hydrogen is converted into the molecular phase (Solomon & Wickramasinghe 1969, Hollenbach et al. 1971, Solomon & Klemperer 1972). The precise molecular gas fraction depends on the intensity of the radiation field, metallicity, and depth into the gas layer. For solar metallicity and low to moderate radiation fields, the gas is expected to be almost fully molecular at column densities greater than 1–2 $\times$ 10^{20} cm^{-2} (Hollenbach et al. 1971, Federman et al. 1979, Sternberg & Dalgarno 1995, Le Petit et al. 2006, Röllig et al. 2006, McKee & Krumholz 2010, Sternberg et al. 2014).

CO molecules are constructed through several different chemical pathways with rates depending on the local temperature and density conditions, far-UV (FUV) radiation field, and gas composition. The primary chemical precursors are CO^+ in the diffuse gas regime and OH in regions of higher gas density (Sheffer et al. 2008, Visser et al. 2009). CO is dissociated by discrete absorption of UV photons to predissociative excited states. Therefore, a shielding layer is also required to attenuate the local radiation field in order to build up a significant abundance of CO. Dust provides the primary opacity element, whereas line opacities from ^{12}CO, ^{13}CO, and H_2 add to the effectiveness of this shielding layer (van Dishoeck & Black 1988, Visser et al. 2009). Detailed photodissociation models with moderate radiation fields demonstrate that much of the C resides within CO at column densities greater than $1–3 \times 10^{21}$ cm^{-2} (Visser et al. 2009). In this column density regime, one can expect CO and its isotopologues to be coextensive with H_2 and a useful tracer of H_2 column density and kinematics. In regions of high volume density and cold dust temperatures, CO can freeze out onto grain surfaces, leading to a reduced CO abundance (Bergin et al. 1995, Acharyya et al. 2007).

Depending on metallicity and the FUV radiation field, the photochemistry models identify a range of column densities over which hydrogen is primarily molecular, yet C resides within its atomic or singly ionized forms rather than CO (Tielens & Hollenbach 1985, van Dishoeck & Black 1988, Sternberg & Dalgarno 1995, Wolfire et al. 2010). Such regions of H_2 without CO could account for much of the so-called dark gas that is revealed by total gas tracers, such as high-energy gamma rays and IR dust emission, but not by the line emissions of CO and HI (Grenier et al. 2005, Planck et al. 2014). However, much of the dark gas could as well be cold, optically thick HI in molecular cloud envelopes (Fukui et al. 2014). Further studies of the dark gas in HI absorption (Dickey et al. 2003), CH and OH emission (Allen et al. 2012), and C^+ emission (Langer et al. 2014) are required before its true nature and distribution can be determined.

The requirement of a shielding layer to attenuate dissociating UV radiation leads to the description of molecular regions as clouds in which there is a clearly defined edge enclosing the dominant constituent of molecular hydrogen and another boundary, interior to the H_2 edge, within which C is locked into CO. Such molecular cloud structures are embedded within envelopes of atomic hydrogen gas that can be traced by the HI 21-cm emission line. Early millimeter observations that mapped the distribution of CO with low sensitivity by today's standards identified spatially discrete units of emission. Many of the early targets for molecular line observations were the patches of visual extinction or dark clouds found by Barnard et al. (1927) and cataloged by Lynds (1962). The term giant molecular cloud (GMC) was applied to regions with H_2 mass in excess of 10^5 $M_\odot$ (Solomon & Edmunds 1980).

Throughout this review, we consider whether this cloud configuration is an appropriate description of molecular regions in the Galaxy in the light of sensitive CO and dust continuum imaging data that reveal complex networks of dense filaments embedded within an extended, diffuse molecular component that frequently links to other distinct regions. Furthermore, no molecular object is strictly isolated, as these are immersed within an atomic substrate that connects to even larger structures in the Galaxy (Hennebelle & Falgarone 2012). This connectedness complicates our observational definition of an interstellar molecular cloud and our ability to identify such features within Galactic plane CO surveys.

An essential requirement to investigate the molecular ISM is the ability to derive the molecular hydrogen gas column density, N_{H_2}. For molecular line measurements of ^{12}CO that resolve the cloud, the H_2 column density is generally determined from the application of the CO-to-H_2 conversion factor, X_{CO}, such that $N_{H_2} = X_{CO} W_{CO}$ cm^{-2}, in which W_{CO} is the ^{12}CO surface brightness integrated over the velocity width of the cloud, $W_{CO} = \int T_B(v) dv$ K km s^{-1}, and

$T_B(v)$ is the ^{12}CO spectrum in units of brightness temperature. There has been an extensive debate on the foundation and accuracy of ^{12}CO as a measure of H_2 column density since the earliest applications of X_{CO} (Bolatto et al. 2013). In nearby clouds, a correlation of integrated ^{12}CO emission and dust extinction does exist in the range of $1 < A_V < 4$ magnitudes but with large scatter (J.E. Pineda et al. 2008, J.L. Pineda et al. 2010, Ripple et al. 2013). In this review, we adopt the value $X_{CO} = 2 \times 10^{20}$ molecules cm^{-2} (K km s^{-1})$^{-1}$ recommended by Bolatto et al. (2013) but also discuss the impact of variations of X_{CO} in the Galaxy.

An alternative estimate of N_{H_2} using ^{13}CO emission requires several steps and assumptions. One can assume optically thin ^{13}CO emission or derive the ^{13}CO opacity, $\tau_{13}(v)$, using the brightness of the optically thick ^{12}CO line, if available, as a measure of the ^{13}CO excitation temperature and then correct the optically thin column density value by the factor $\int \tau_{13}(v)dv / \int [1 - \exp[-\tau_{13}(v)]]dv$ and a second factor that depends only on T_{ex} and the background temperature, T_{bg} (J.L. Pineda et al. 2010). A constant excitation temperature is assumed to estimate the fractional population in all J levels of ^{13}CO. In the low-density regime of molecular clouds, the $J = 1$–0 excitation temperature of ^{13}CO is often smaller than the value determined from ^{12}CO. By adopting the excitation temperature of ^{12}CO, which is higher than the appropriate, subthermal value, the resultant ^{13}CO column density is underestimated. Finally, to derive H_2 column density, an isotopic ratio of ^{12}CO/^{13}CO and H_2/^{12}CO abundance ratio are assumed. Based on H_2 and CO IR absorption lines, the H_2/CO abundance ratio ranges from 4,000 to 7,000 (Lacy et al. 1994, Kulesa 2002). However, both isotopic and CO abundance ratios can vary within clouds and from cloud to cloud owing to isotopic fractionation and local UV fields.

For nearby clouds, dust extinction and dust emission methods provide a more accurate measure of H_2 column density than does CO spectroscopy. However, at distances greater than several kiloparsecs in the Galactic plane, the dust techniques are limited by foreground and background contamination. For all its limitations and required assumptions, CO remains the primary measure of molecular cloud mass throughout most of the Galaxy.

3. CARBON MONOXIDE SURVEYS OF THE MILKY WAY

Surveys aren't the most important thing in astronomy—they're the only thing. —J. Ostriker

The $J = 1$–0 line of ^{12}CO is nearly as important for studying the molecular gas in the Galaxy as the 21-cm line is for atomic gas. No other molecule has the combination of high abundance and low dipole moment necessary to produce strong emission lines from most of the molecular gas in the Galaxy. CO observations are so ubiquitous that molecular clouds are often referred to as CO clouds, and the previous review in this volume on Galactic molecular clouds was titled "The Distribution of CO in the Milky Way" (Combes 1991). Much of what we know about the general properties and Galactic distribution of molecular clouds comes from analysis of the relatively small number of unbiased CO plane surveys discussed here. These well-documented and widely available surveys provide large samples of clouds for assessing both mean properties and how these properties may vary with Galactic environment.

CO surveys are important not only for studying molecular clouds directly but for interpreting the Galactic emission at almost every other wavelength band. Molecular clouds produce much of the diffuse gamma-ray emission (Ackermann et al. 2012) and absorb the diffuse X-ray background (Wang & Yu 1995), and they are seen as dark nebulae in the optical and near-IR (Lombardi et al. 2011). Dust in molecular clouds is responsible for a substantial fraction of the Galactic far-IR emission (Planck Collaboration XXIII et al. 2014) and millimeter wave continuum (Schuller et al. 2009, Aguirre et al. 2011). Massive star formation within molecular clouds produces masers

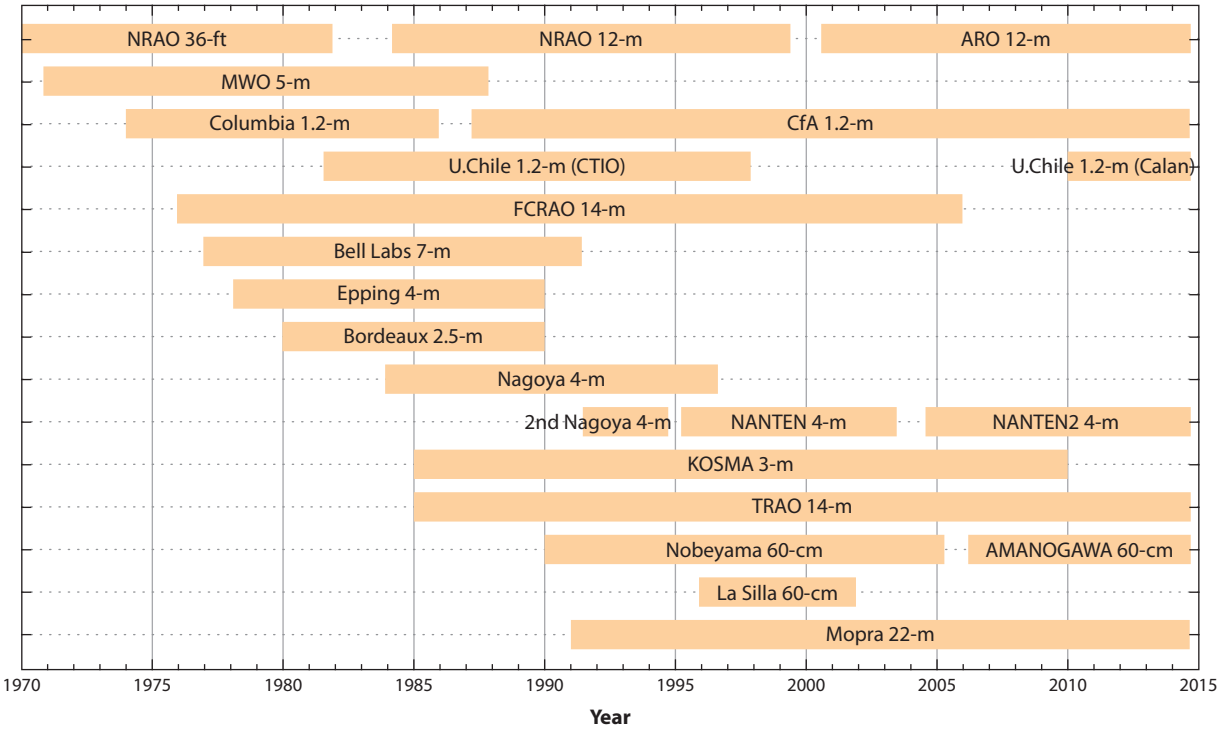

Figure 1

A summary of single-dish telescopes that have conducted large carbon monoxide surveys of the Milky Way. These are sorted top to bottom by the year of their first observations, with the exception that twin telescopes located in opposite hemispheres are grouped together. Changes of a telescope's location, institution, aperture, or operating frequency are marked by breaks in the horizontal lines.

and prominent sources of radio continuum, IR, X-ray, and TeV gamma rays. Moreover, the CO surveys provide crucial kinematic information that is often the only handle on the distances to the diffuse emission and sources observed at other wavelengths. Considering also their importance in studying spiral structure, Galactic surveys in CO arguably have a broader range of applicability than those at any other wavelength.

Single-dish millimeter and submillimeter telescopes have produced multiple large or historically significant surveys of the Galactic plane and important nearby clouds, such as Orion and Taurus. Such surveys are best done with telescopes of moderate aperture that can be dedicated to the task for long periods of time. **Figure 1** lists the telescopes that have carried out significant surveys of CO emission and indicates the time periods over which each was operational.

3.1. Galactic Plane Surveys

Large CO surveys of the Galactic plane since the discovery of the CO line in 1970 are summarized in **Figure 2**. Large is defined here as an area >10 deg^2 or a strip of observations more than 5° along the Galactic plane. Although unorthodox, this figure reveals a great deal about the number, size, type, and quality of surveys over the Galactic plane and over time. It is clear, for example, that the first quadrant has been surveyed most extensively and sensitively and that it was over 20 years before much of the third quadrant was surveyed at better than 0.5° angular resolution. Here, we discuss chronologically just a few of the surveys of particular interest.

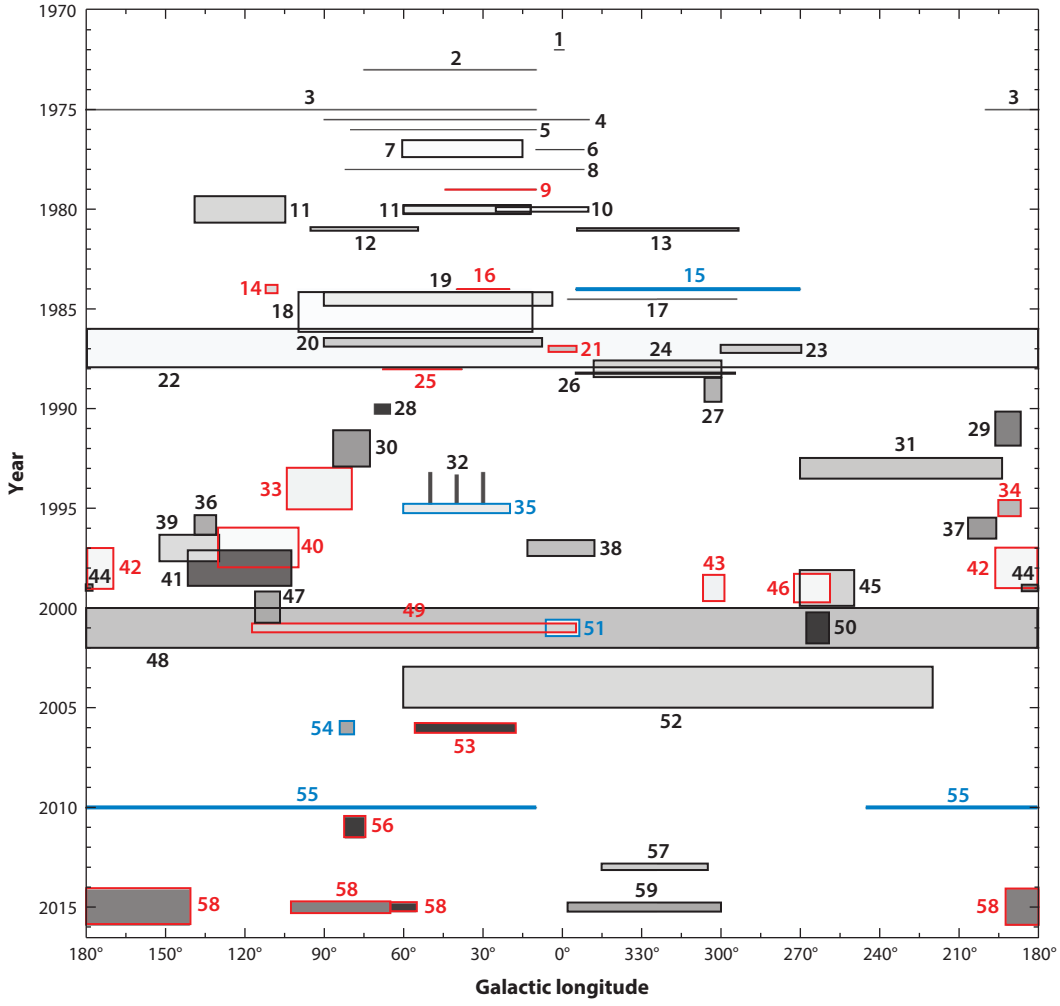

Figure 2

A summary of large CO surveys of the Galactic plane. The numbers are keys to each survey's publication listed at the end of this caption. The limits of each survey are approximated by a rectangle that is positioned vertically at the year of its publication. For clarity, the maximum value of $|b|$ for all surveys is limited to 5°. Surveys outlined in red are in the ^{13}CO line and those in blue are in the ^{12}CO (2–1) line. The grayscale shading indicates sensitivity per unit area and velocity interval; specifically, it indicates the root mean square (rms) at 1 km s^{-1} spectral resolution that one would obtain by averaging all survey spectra within 1 deg^2. The rms sensitivities for ^{13}CO surveys are increased by a factor of five to account for the reduced intensity of that line. The grayscale runs from ∼0.01 K rms (*black*) to ∼10 K rms (*white*). 1, Solomon & Klemperer 1972; 2, Schwartz et al. 1973; 3, Burton et al. 1975; 4, Scoville & Solomon 1975; 5, Gordon & Burton 1976; 6, Bania 1977; 7, Cohen & Thaddeus 1977; 8, Burton & Gordon 1978; 9, Solomon et al. 1979; 10, Bania 1980; 11, Cohen et al. 1980; 12, Kutner & Mead 1981; 13, McCutcheon et al. 1981; 14, Casoli et al. 1984; 15, Israel et al. 1984; 16, Liszt et al. 1984; 17, Robinson et al. 1984; 18, Dame & Thaddeus 1985; 19, Knapp et al. 1985; 20, Sanders et al. 1986; 21, Bally et al. 1987; 22, Dame et al. 1987; 23, Grabelsky et al. 1987; 24, Bronfman et al. 1988; 25, Jacq et al. 1988; 26, Robinson et al. 1988; 27, Nyman et al. 1989; 28, Digel et al. 1990; 29, Stacy & Thaddeus 1991; 30, Leung & Thaddeus 1992; 31, May et al. 1993; 32, Dame & Thaddeus 1994; 33, Dobashi et al. 1994; 34, Carpenter et al. 1995; 35, Sakamoto et al. 1995; 36, Digel et al. 1996; 37, Oliver et al. 1996; 38, Bitran et al. 1997; 39, Sato 1997; 40, Yonekura et al. 1997; 41, Heyer et al. 1998; 42, Kawamura et al. 1998; 43, Kato et al. 1999; 44, Lee et al. 1999; 45, Yamaguchi et al. 1999; 46, Yamaguchi et al. 1999; 47, Ungerechts et al. 2000; 48, Dame et al. 2001; 49, Lee et al. 2001; 50, Moriguchi et al. 2001; 51, Sawada et al. 2001; 52, Mizuno & Fukui 2004; 53, Jackson et al. 2006; 54, Schneider et al. 2006; 55, Yoda et al. 2010; 56, Schneider et al. 2011; 57, Burton et al. 2013; 58, Brunt et al. 2015; 59, Barnes et al. 2015.

The earliest surveys of the plane (Nos. 1–6, 8, 9 in **Figure 2**), all carried out with the NRAO 36-ft telescope, were poorly sampled strips of observations at or very near the Galactic plane. These were adequate to show that molecular gas was extensive in the Galactic Center (**Figure 2**, Nos. 1 and 6) and in the inner Galaxy (**Figure 2**, Nos. 2–5) and that the radial distribution of H_2 was distinctly different from that of HI, strongly peaking about half-way between the Sun and the Galactic Center in what was soon dubbed the molecular ring. The first out-of-plane survey (**Figure 2**, No. 7) showed that H_2 was distinct from the HI in its vertical distribution as well, being more confined to the plane by roughly a factor of two, but was similar to the HI in showing ripples about the mid-plane with an amplitude of a few tens of parsecs.

The first ^{13}CO plane survey (No. 9 of **Figure 2**) was important for showing that the distribution of H_2 as derived from this line was, quite surprisingly, not significantly different from that derived from the much higher opacity CO line. To first order, the ^{13}CO spectra along the plane looked like lower signal-to-noise versions of the corresponding ^{12}CO spectra. This led to the supposition, still held today, that on large scales the CO line is essentially counting optically thick clouds or clumps with similar average properties within molecular clouds and across the Galaxy.

The large survey, No. 18 in **Figure 2**, was the first to employ a relatively simple software technique on the 1.2-m telescopes that allowed very large areas to be well sampled very rapidly. In the case of that survey, the telescope was offset through a square 8×8 raster of points separated by 0.125° (approximately one beamwidth) during a typical few-minutes observation. The data from all 64 positions were accumulated into a single spectrum that closely approximated what would be obtained with a 1° beam. This early technique bore some resemblance to modern-day on-the-fly mapping in that the telescope was moved almost continuously during observations and multiple on-source positions were observed for each off-source measurement.

Many more such superbeam surveys, most with an effective angular resolution of 0.5°, were conducted with the 1.2-m telescopes during the early and mid-1980s. These allowed the first well-sampled survey of the entire Milky Way to be compiled in 1987 (No. 22 of **Figure 2**) many years before it otherwise would have been possible. In addition to being widely used for studies of star formation and Galactic structure, the survey proved essential for interpreting the diffuse Galactic gamma-ray emission observed by the SAS *(Small Astronomy Satellite)*-2 (Arnaud et al. 1982), Cos-B (Bloemen et al. 1986), and EGRET (*Energetic Gamma Ray Experiment Telescope;* Hunter et al. 1997) satellites, particularly because the 0.5° resolution of the CO survey exceeded that of all three gamma ray surveys. Such gamma-ray analyses yielded insights into the Galactic cosmic-ray distribution as well as a Galaxy-wide calibration of the CO-to-H_2 conversion factor.

Even before the superbeam surveys were undertaken, the twin 1.2-m telescopes were conducting surveys at several times higher angular resolution—typically every beamwidth but sometimes half or twice that. By 2001 these surveys could be combined into a new composite survey of the Galaxy with up to 10 times higher sensitivity per unit area (No. 48 of **Figure 2**). This survey remains the most extensive and widely used census of Galactic molecular gas, particularly because all the component surveys and the full composite survey are publically available online as raw, interpolated, and noise-suppressed data cubes (**http://www.cfa.harvard.edu/rtdc/CO/**).

Another composite CO survey was compiled from observations conducted by the NANTEN 4-m telescope at Las Campanas observatory between 1996 and 2004 (No. 52 of **Figure 2**). The full survey extends from longitude 220° through the Galactic Center to longitude 60° and consists of over 1.1 million spectra. Compared with the 1.2-m composite survey, the NANTEN survey provides a factor of two better angular resolution near the plane (4-arcmin spacing at $|b| < 5°$) and roughly the same sensitivity per unit area and velocity interval. At higher latitudes the effective angular resolution is comparable (8-arcmin spacing) and the sensitivity per unit area is a factor of two lower.

The Five College Radio Astronomy Observatory (FCRAO) 14-m telescope has also made important contributions to the mapping of CO emission in the Milky Way. The University of Massachusetts–Stony Brook (UMSB) survey of the first quadrant (No. 20 of **Figure 2**) was widely used for studies of the molecular gas distribution in the inner Galaxy ($R_{GAL} < 8.5$ kpc) and the properties of molecular clouds (Solomon et al. 1987). With its pioneering development and application of heterodyne focal plane arrays, FCRAO carried out an imaging survey of ^{12}CO $J = 1$–0 emission from the outer Galaxy (No. 41 of **Figure 2**), the Boston University-FCRAO Galactic Ring Survey (GRS) of ^{13}CO $J = 1$–0 emission (No. 53 of **Figure 2**), and simultaneous imaging of both ^{12}CO and ^{13}CO emission from longitudes 56° to 102° and 140° to 192° with varying latitude coverage (No. 58 of **Figure 2**). The sensitivity and high angular and spectral resolutions of these surveys enable views of the internal density and velocity structure of molecular clouds and offer a powerful complement to the lower-resolution but wider-field perspectives of CO emission observed with the twin 1.2-m and Nagoya/NANTEN systems.

3.2. High-Latitude Surveys

Here, we discuss observations of molecular gas lying more than 25° from the Galactic plane, a common definition of the high-latitude sky. Obvious difficulties in finding molecular gas in this region include the enormous area involved, the generally low column densities of all gas and dust at large angles from the plane, and the relatively low stellar background against which dark clouds must be spotted. We first discuss targeted surveys toward regions of obscuration and IR emission and then discuss the few unbiased surveys that have been completed or are under way.

3.2.1. Targeted surveys toward high-latitude clouds. The first few detections of molecular clouds at high latitude were the results of observations not focused specifically on that region. In particular, Dickman (1975) searched for CO toward 64 dark clouds in the Lynds (1962) catalog and detected all but one; among his detections were 7 dark cloud complexes in the range of $|b| = 25°$–$37°$ (Magnani 1994). Similarly, Blitz et al. (1982) surveyed CO toward optical HII regions, most from the catalog of Sharpless (1959), and detected 6 dark clouds at $|b| > 25°$. In addition, a search for OH absorption toward 58 extragalactic radio sources yielded 2 detections at $|b| > 25°$ (Dickey et al. 1981), and a search for CO toward extragalactic sources showing strong 21-cm absorption by Kazès & Crovisier (1981) yielded 4 high-latitude detections, 2 of which were already detected by Dickey et al. (1981).

This relatively small number of molecular cloud outliers more than 25° from the plane did little to change the view that the high-latitude sky was largely devoid of molecular gas. It was rather surprising, therefore, when Blitz et al. (1984) scoured the Palomar Observatory Sky Survey plates for regions of obscuration at high latitudes and subsequently detected CO at nearly one quarter of the 457 candidate regions observed. These detections resulted in the publication one year later of the well-known MBM catalog of high-latitude molecular clouds (Magnani et al. 1985), which contains 57 clouds in 35 complexes. Keto & Myers (1986) followed up with a similar survey of the southern sky, using obscuration on the European Southern Observatory sky plates as their guide and adding 8 new clouds at $|b| > 25°$.

Another tracer of molecular gas at high latitude was provided by the *Infrared Astronomical Satellite* (IRAS), which discovered diffuse, highly structured far-IR emission over essentially the entire sky (Low et al. 1984). Most prominent at 60 and 100 μm, this so-called IR cirrus was shown by Boulanger et al. (1985) to be well correlated with 21-cm line emission at high latitudes, suggesting that the cirrus emission arose from dust uniformly mixed with the interstellar gas and uniformly heated. Soon thereafter, Desert et al. (1988) compiled a catalog of so-called IR excess

clouds (IRECs), regions in which the far-IR emission was stronger than expected from the known amount of HI, perhaps owing to the existence of molecular gas there. An updated catalog of IRECs was derived by Reach et al. (1998) based on improved IR data from the *Cosmic Background Explorer* (COBE; Boggess et al. 1992) and improved 21-cm data from the Leiden-Dwingeloo survey (Hartmann & Burton 1997).

It remains unclear what fraction of the IRECs are molecular. A search by Blitz et al. (1990) for CO from 201 IRECs in the Desert et al. (1988) catalog detected only 13%, whereas similar searches by Onishi et al. (2001) and Chi & Park (2006) based on the Reach et al. catalog yielded CO detection rates of 47% and 21%, respectively. Blitz et al. (1990) proposed that the IRECs not detected in CO are regions of diffuse H_2 with CO abundances too low to detect. Although this is plausible, it remains difficult to rule out other possibilities, such as variations in the gas-to-dust ratio, dust properties, or dust temperature, and varying 21-cm optical depth.

3.2.2. Unbiased surveys for high-latitude clouds. The first unbiased CO survey at high latitudes was carried out by Magnani et al. (1986) specifically to determine the completeness of the MBM cloud catalog (Magnani et al. 1985). Had the dust obscuration used by MBM to find high-latitude clouds revealed most of them, or just a small fraction? To address this question, roughly two dozen $10° \times 10°$ regions well distributed around the sky were mapped with 1° sampling in Galactic longitude and latitude. The results suggested that the MBM catalog was about half complete, which in turn implied that high-latitude clouds within 100 pc of the Sun had a total mass of $\sim$5,000 $M_\odot$ and contributed $\sim$0.2 $M_\odot$ pc^{-2} to the local molecular mass surface density.

The first unbiased CO survey of the entire northern high-latitude sky ($\delta > -17.6°$) was carried out with the Center for Astrophysics (CfA) 1.2-m telescope by Hartmann et al. (1998) at $b > 30°$ and Magnani et al. (2000) at $b < -30°$. A total of 15,544 positions were observed on a 1° true-angle grid using an innovative ON-minus-ON position-switching between two positions in the observing grid separated by 1° in latitude. Except in the unlikely event that emission is present at both positions with the same intensity and velocity, such switching reveals emission at either position as a positive or negative line in the difference spectrum. When such features appeared, both positions were observed more sensitively using frequency switching to obtain the true line profiles. One drawback of this technique was that it yielded simply a catalog of detections rather than a conventional spectral line data cube from which sky maps could be produced. The survey discovered CO at 60 new locations, 2 at $b > 30°$ and the rest at $b < -30°$, an asymmetry consistent with that found in previous studies.

Not long after publication of the composite CO survey of the Galaxy by Dame et al. (2001), a new survey with the CfA 1.2-m telescope was begun with the goal of observing all of the area at $|b| < 30°$ not covered by the Dame et al. survey; the sampling was every 1/4° or roughly every other beam width (Dame & Thaddeus 2004). Even after achieving this goal, the survey was continued over the years until the entire northern sky was completed in the spring of 2014. Compared with the previous survey by Magnani et al. (2000) just discussed, this new survey has four times higher angular resolution and sensitivity per unit area. Moreover, the survey employed conventional frequency switching, which allows for the construction of data cubes and sky maps. Although some data processing remains, a preliminary map derived from the new CfA northern sky survey is shown in **Figure 3**; it is combined with both the Dame et al. (2001) composite survey of the plane and a similar composite from the NANTEN telescope (Mizuno & Fukui 2004). This map represents all major Galactic CO surveys to date.

Finally, it is worth mentioning the all-sky CO maps recently extracted as "foreground contamination" from the Planck survey data (Planck Collaboration et al. 2014). Planck observes the sky in nine frequency bands covering 30–857 GHz primarily to study the temperature and

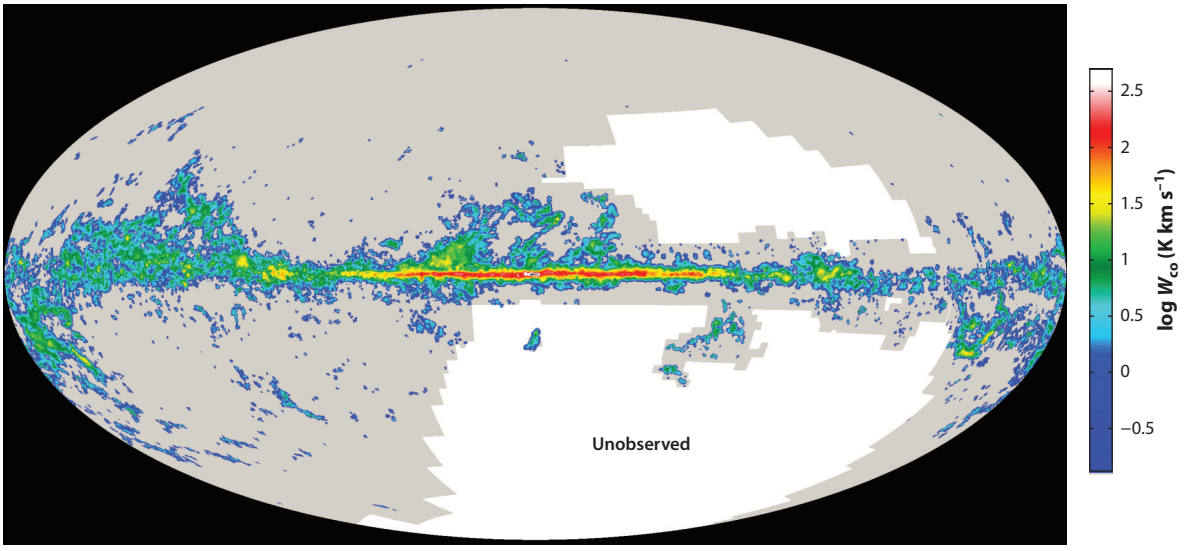

Figure 3

An image of ^{12}CO $J = 1$–0 emission constructed from the recent Center for Astrophysics campaign to examine the high-latitude sky and the composite surveys of Dame et al. (2001) and Mizuno & Fukui (2004).

polarization anisotropies of the cosmic microwave background. The highest six of these bands are observed with bolometers cooled to 0.1 K. Remarkably, these instruments are so sensitive that the three lowest rotational transitions of CO are detectable even though the widths of these lines are several orders of magnitude narrower than the bandwidth of the bolometers. Three different extraction schemes were used to derive CO sky maps with different trade-offs in terms of angular resolution, sensitivity, and systematics. The best angular resolution achieved was 5 arcmin and the best sensitivity was shown to be comparable with that of the Magnani et al. (2000) high-latitude survey. Although agreement with existing CO surveys is generally quite good, the Planck CO maps still suffer from some level of contamination from dust, other CO lines (especially ^{13}CO), and the Sunyaev-Zel'dovich effect. More importantly, they lack the kinematic information that is so important for interpreting the Galactic emission at many other wavelengths.

4. THE DISTRIBUTION OF MOLECULAR GAS IN THE GALAXY

I don't believe any spiral arm until I see it in the l-v diagram. —R. Benjamin

The molecular phase of the ISM offers distinct advantages over the atomic phase for determining its Galactic distribution. Most of the Galactic H_2 mass is contained in the large GMCs (Section 5.1.3), which are generally far better defined than atomic clouds and can be detected and resolved throughout the Galaxy even with a 1-m dish. These objects have a lower cloud-cloud velocity dispersion than atomic clouds and, therefore, lower uncertainties on kinematic distances, and they are associated with a wealth of Population I objects, which are useful in resolving the kinematic distance ambiguity.

The main challenges for determining the molecular distribution are the kinematic distance ambiguity within the solar circle, noncircular motions induced both locally by stellar winds and supernovae and on a Galactic scale by density waves and the Galactic bar, and identifying,

categorizing, and resolving the distance ambiguity for the large number of sub-GMC-class clouds that blend into a near continuum of CO emission.

In Sections 4.1–4.3, we discuss the main methods that have been employed to determine the Galactic distribution of molecular gas. The distribution as it relates to the Galactic spiral structure is discussed specifically in Section 4.4, the vertical distribution is discussed in Section 4.5, and Section 4.6 provides an estimate of the total molecular mass of the Galaxy.

4.1. Axisymmetric Modeling

With the Galactic rotation curve known and circular orbits assumed, the Galactic radius corresponding to each spectral channel in a CO survey can be calculated unambiguously. It is therefore straightforward in principle to determine the average radial distribution of CO emission. For an analysis at $b = 0$, the emission can simply be averaged in radial bins with a weighting that accounts for the nonlinear relationship between velocity and distance along each line of sight. Analyses of this sort were first carried out in the first quadrant by Burton et al. (1975) and Scoville & Solomon (1975) and in the fourth quadrant by Robinson et al. (1984).

For the analysis of an out-of-plane CO survey, the Galaxy can be modeled as a series of concentric rings, each characterized by a central CO emissivity, a vertical (z) thickness, and an offset from $z = 0$. The three best-fit parameters for each ring can be converted to an H_2 mass surface density by integrating the CO emissivity over z and applying the CO-to-H_2 mass conversion factor, X_{CO}. This is the approach adopted by Sanders et al. (1984) for an analysis of the UMSB CO survey and by Bronfman et al. (1988) for analysis of the Center for Astrophysics–University of Chile (CfA–U.Chile) CO survey. Although these two analyses were basically similar and "straightforward in principle," they yielded H_2 mass surface densities and total H_2 masses within the solar circle that differed by more than a factor of two.

Bronfman et al. (1988) were able to show that this difference could be attributed to three factors all biasing the UMSB results above those of the CfA–U.Chile group: an X_{CO} difference of 1.3, different weighting schemes resulting in a factor of 1.4, and a CO intensity calibration difference of 1.2. The X_{CO} factors adopted by both groups were well above the value 2×10^{20} cm^{-2} (K km s^{-1})$^{-1}$ currently thought to apply to most of the H_2 in the Galaxy (Bolatto et al. 2013). The weighting scheme of UMSB assigned equal weights to lines of sight with very different sampled path lengths and, as Bronfman et al. (1988) showed, yielded results that substantially overpredicted the CO integrated intensity versus longitude. Regarding the calibration of the CfA survey, it has been so widely used for calibrating the average Galactic X factor with both gamma rays (Strong & Mattox 1996, Ackermann et al. 2012) and dust emission (Dame et al. 2001, Planck Collaboration XIX et al. 2011) that it has become the de facto standard.

The analysis by Bronfman et al. (1988) remains the only valid axisymmetric unfolding of an out-of-plane CO survey covering both the first and fourth Galactic quadrants. Because both the sensitivity and angular resolution of the CfA survey are more than adequate for the purpose, the Bronfman et al. (1988) results are likely to remain the final word for this approach for some time, although care must be taken in correcting their results for the solar Galactic radius (they used 10 kpc) and X_{CO} [they used 2.8×10^{20} cm^{-2} (K km s^{-1})$^{-1}$]. The axisymmetric results so corrected are presented in Section 4.6 to estimate the total H_2 mass of the Galaxy.

4.2. "Double Gaussian" Approach

A first step beyond the assumption of axial symmetry for determining the molecular gas distribution is provided by a technique that dates from the earliest days of Galactic 21-cm astronomy (Schmidt

1956). Its underlying assumption is that the emitting gas fills a layer of roughly constant thickness so that, at each longitude and velocity corresponding to positions within the solar circle, two roughly Gaussian layers with different widths in latitude can be identified—one originates from the near kinematic distance and the other from the far. Because the analysis essentially consists of fitting these layers at each (l,v) location with a double Gaussian or comparable function to distribute the emission near/far, we refer to the technique as the double Gaussian approach.

An advantage of this technique, which it shares with axisymmetric modeling, is that it distributes essentially all the observed CO emission into the Galactic plane (albeit not always correctly) and thus can yield an estimate of the total Galactic CO luminosity and H_2 mass. However, the technique is clearly better suited for the atomic gas for which it was originally developed. The atomic gas essentially fills the Galactic plane with relatively low contrast between cloud and intercloud regions, whereas the molecular gas is mainly concentrated in large, clumpy clouds that are subject to being incorrectly partitioned into near and far components by the double Gaussian fit. The net result of many such erroneous partitions between two positions at the same radius is a tendency toward rings in the derived gas distribution.

This technique has been applied to the UMSB CO survey of the first quadrant by Clemens et al. (1988) and to the entire CfA-U.Chile CO survey of the Galaxy by Nakanishi & Sofue (2006). In both analyses, the CO emission was analyzed over fairly large bins in velocity and longitude (roughly 6 km s^{-1} by 2°) to smooth out the influence of single molecular clouds. Of course, such smoothing also degrades the resolution of the derived density distributions. These results are discussed and compared with the results of other methods in Section 4.4.

Another far more ambitious attempt to deconvolve the entire CfA-U.Chile CO survey by Pohl et al. (2008) is essentially based on the double Gaussian approach in that emission is distributed along the line of sight mainly by latitude. However, in their analysis highly noncircular motions based on bar-driven gas flow simulations result in up to eight possible kinematic distances along any line of sight. The liability of using such a complicated velocity field is that any deviation from the true velocity field introduces equally complicated distortions in the inferred gas distribution.

4.3. Cloud-by-Cloud

The two techniques so far discussed do not take advantage of the unique aspects of the molecular gas, i.e., its concentration into large GMCs with relatively low velocity dispersion and a wealth of associated Population I objects. To do so, one must identify GMCs within CO surveys and determine their physical properties. Although this is fairly straightforward in the outer Galaxy, where GMCs are generally few and far between, the inner Galaxy presents considerable challenges owing to the distance ambiguity and cloud blending, which is particularly severe near the terminal velocity in each direction.

Until just the past few years, the only published inner-Galaxy molecular cloud catalogs were those of Dame et al. (1986), Scoville et al. (1987), and Solomon et al. (1987), all covering only the first Galactic quadrant. Dame et al. (1986) used the Columbia CO survey to identify the largest GMCs after subtracting an axisymmetric background from the data. Both Scoville et al. (1987) and Solomon et al. (1987) used the UMSB CO survey and defined clouds as topologically closed surfaces of antenna temperature in l-b-v space; the defining temperature was chosen somewhat differently by the two groups to stay above the underlying background emission.

The severity of the cloud blending that presumably produces the background emission is evidenced by the fact that the total mass of clouds in each of the three catalogs is less than 20% of the total mass determined to be in the observed region by axisymmetric model fitting of the same surveys. Williams & McKee (1997) used all three catalogs to calibrate the molecular cloud

mass spectrum, which is well determined by the catalogs at the high-mass end, and subsequently integrated the spectrum over all clouds to obtain a total mass ~40% of that of the axisymmetric fit. Solomon & Rivolo (1989) argued that the mass not in the cloud catalogs resides within relatively cold unidentified clouds. It is also possible that the axisymmetric model fits have overestimated the total H_2 mass owing to large nonaxisymmetric features in the cloud distribution (Dame 1993).

Since the early works just discussed, a wealth of new data and techniques have become available for resolving the kinematic distance ambiguity. Most important are the high-resolution interferometric 21-cm surveys that now cover the inner Galaxy in the first quadrant [the Very Large Array (VLA) Galactic Plane Survey or VGPS; Stil et al. 2006] and the fourth quadrant (Southern Galactic Plane Survey or SGPS; McClure-Griffiths et al. 2005). These surveys allow the ambiguity to be resolved for the majority of inner Galaxy GMCs from either HI self-absorption produced by the cloud itself or foreground absorption against associated continuum sources (Roman-Duval et al. 2009). The blending problem too has been mitigated somewhat by the completion of the GRS in the first quadrant (No. 53 in **Figure 2**), which provides high angular and velocity resolution and unprecedented sensitivity in the ^{13}CO line, which is less subject to blending owing to its lower optical depth.

With these new techniques and data in hand, Rathborne et al. (2009) used the automated algorithm CLUMPFIND (Williams et al. 1994) to identify 829 clouds in the GRS, and Roman-Duval et al. (2009) used the VGPS to resolve the kinematic distance ambiguity for most of these. Roman-Duval et al. (2010) studied their physical properties and Galactic distribution. Also of note is the recent completion of the first census of molecular clouds in the fourth quadrant, which is based on the CfA-U.Chile CO survey (García et al. 2014). For further progress in this area, surveys comparable with the GRS in resolution and sensitivity in the fourth quadrant are required. There are currently two surveys being undertaken with the Mopra telescope that may be suitable (Nos. 57 and 59 in **Figure 2**).

Beyond the solar circle where cloud blending is minimal and the distance ambiguity is nonexistent, the main difficulty in studying clouds is the very large area that must be observed, particularly owing to the flaring and warping of the outer disk (see Section 4.5). The only unbiased study of the entire outer Galaxy is that by Sodroski (1991), who used the preliminary whole-Galaxy CO survey conducted by Dame et al. (1987) to identify 35 molecular clouds; however, this study was limited by the low angular resolution of the survey, ~0.5°. Rather than rely on a uniform survey, Wouterloot & Brand (1989) observed CO toward 1,302 IRAS sources in the outer Galaxy with colors indicative of star-forming regions; many of these clouds were later mapped by Brand & Wouterloot (1994). Other outer Galaxy cloud studies have been confined either to particular spiral arms (see below) or to the area of the FCRAO Outer Galaxy survey (Heyer et al. 2001, Brunt et al. 2003).

4.4. Spiral Structure

Efforts to determine the spiral structure of the Milky Way from 21-cm surveys were largely derailed in the 1970s by the demonstration that much or all the apparent spiral structure seen in 21-cm longitude-velocity diagrams could just as well be produced by large-scale, low-amplitude streaming motions as by genuine arm-interarm density contrast in the atomic gas (Burton 1971). The impact of this work still reverberated as the early CO surveys of the inner Galaxy were analyzed a decade later, and it led some to propose that spiral-like features in the CO were likewise little more than kinematic illusions (Liszt & Burton 1981). However, sensitive, high-resolution CO and 21-cm observations of the inner Galaxy (see **Figure 4**) have since revealed that the contrast of the CO spiral features is generally far higher than that of HI and far higher than could be produced by

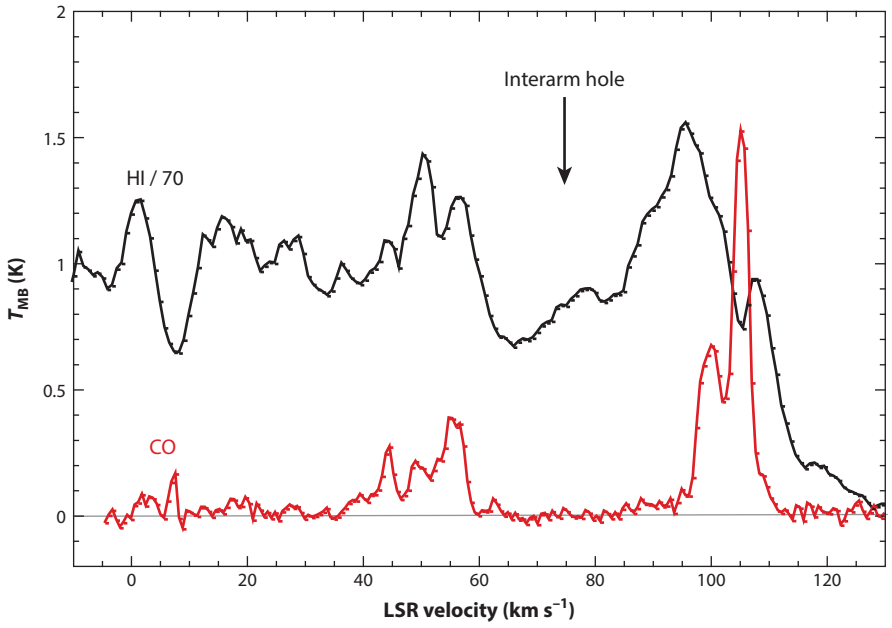

Figure 4

^{13}CO $J = 1$–0 and 21-cm spectra with comparable angular resolutions (~1 arcmin) toward a prominent interarm region in the inner Galaxy (Shane 1972, Dame et al. 1986, Sato et al. 2014) at $l = 25°$, $b = 0°$. ^{13}CO is from the Galactic Ring Survey (Jackson et al. 2006) and HI from the Very Large Array Galactic Plane Survey (Stil et al. 2006). Abbreviation: LSR, local standard of rest.

plausible streaming motions. Recent interferometric observations of external spirals, such as M51 (Schinnerer et al. 2013), likewise leave no doubt that molecular clouds are strongly concentrated to the spiral arms.

Attempts to map the Galactic spiral structure with CO have mainly followed one of two approaches. The most common is based on studying the H_2 gas or cloud distribution in the Galactic XY plane, as derived from either the double-Gaussian or cloud-by-cloud methods. The alternative is to identify and model the characteristic emission patterns of spiral arms in the CO l-v diagram.

Mapping the spiral structure in the XY plane using molecular clouds has been quite successful for the more well-defined spiral arms, including Sagittarius and Scutum in the first quadrant (Dame et al. 1986, Solomon & Rivolo 1989, Roman-Duval et al. 2010) and Carina (Grabelsky et al. 1988), Centaurus, and Norma in the fourth (García et al. 2014). However, it should be kept in mind that the derived XY plane is two complex transformations removed from the true Galactic distribution: a highly nonlinear and in some regions double-valued transformation to the observed l-v diagram, then a second transformation back to XY based on assumed kinematics and, in the inner Galaxy, resolution of the distance ambiguity. Combes (1991) demonstrated how this double transformation can all but wash out the apparent spiral structure of even a grand design galaxy such as M51.

With that caveat in mind, we present in **Figure 5** a comparison of XY maps of the inner first quadrant: three from cloud catalogs, two from the double Gaussian approach, and one from the HII region catalog by Anderson et al. (2012). Several prominent features are evident in most of the maps. The Sagittarius arm (*red*) is seen clearly in all three of the cloud maps as well as in the HII

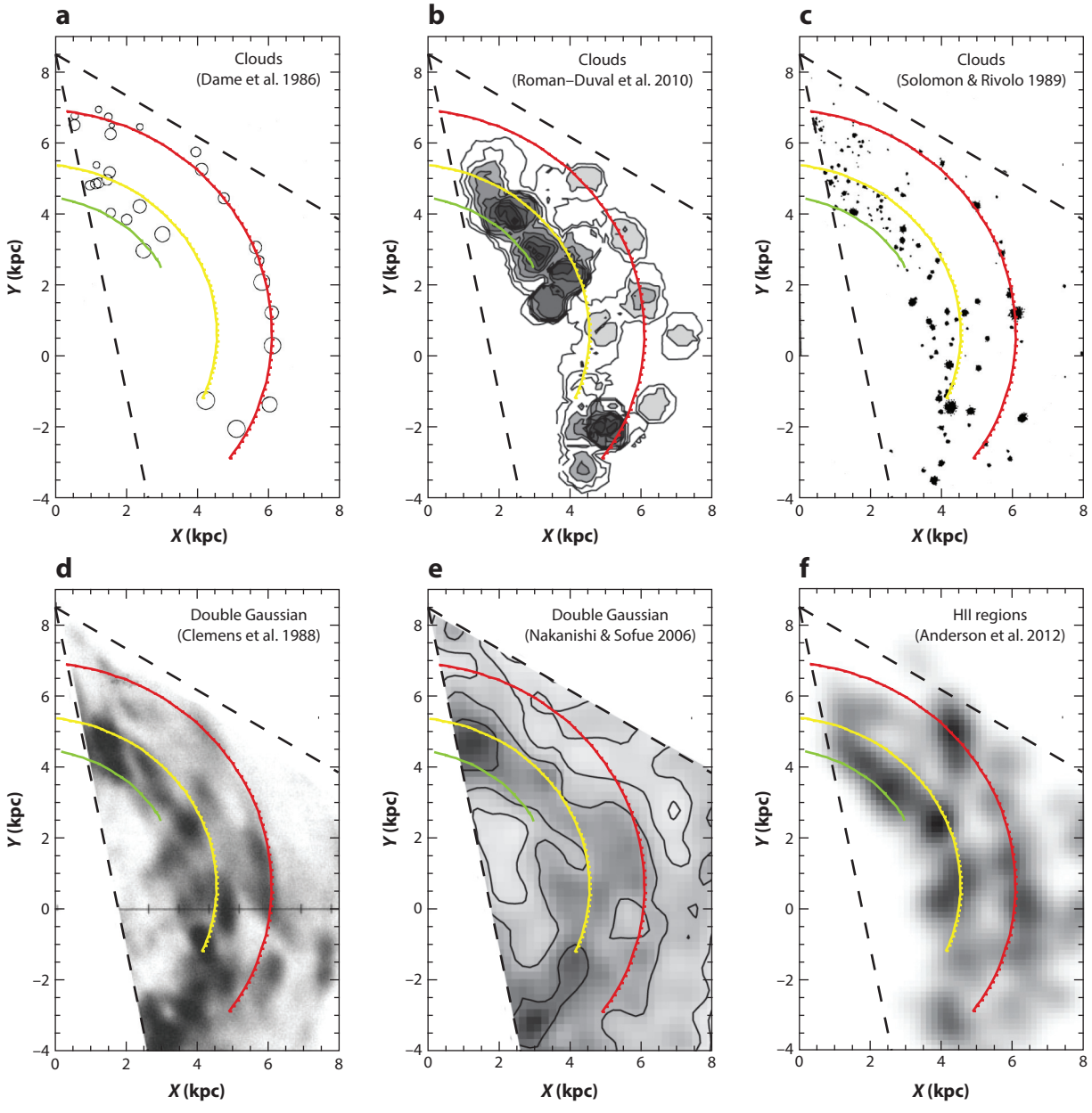

Figure 5

(*a–c*) Maps of the molecular gas distribution in the first Galactic quadrant as derived from cloud catalogs and (*d*,*e*) the double Gaussian approach. For comparison, panel *f* shows the average number density of HII regions (Anderson et al. 2012). To aid comparison, all the maps have been trimmed to a common longitude range and three spiral features overlaid: Norma arm (*green*), Scutum arm (*yellow*), and Sagittarius arm (*red*). Figures are adapted from the cited papers and reproduced with permission from AAS and Oxford University Press.

region map; the arm may be so thin that it is not well resolved by the double Gaussian analyses. Also common to all the maps is prominent emission on the near side of the inner Galaxy, near the start of the Norma arm (*green*). This is widely believed to be gas and star formation trailing off the near side of the central bar. The majority of the maps also suggest some strengthening of the Sagittarius arm on its far side as it spirals inward.

An alternative or complement to XY studies is modeling of the CO l-v diagram, which is as raw a view of the Galactic gas distribution as one can obtain from our perspective in the plane. If a putative spiral feature is not evident in the l-v diagram, defining it only by connecting the dots in the derived XY plane is tantamount to spotting patterns in the wallpaper. One of the most successful early l-v modeling efforts was that by Fux (1999), who used self-consistent N-body simulations to reproduce some of the most prominent and puzzling features of the inner Galaxy, including the Connecting Arm, the Expanding 3-kpc Arm, and the +135 km s^{-1} arm. Similar efforts over the entire inner Galaxy have been presented by Englmaier & Gerhard (1999) and Dobbs & Burkert (2012), and recently over the entire Galaxy by Pettitt et al. (2014).

These models and even much simpler ones (Dame 1983, Combes 1991) demonstrate that the inner-Galaxy l-v diagram can be filled with CO emission to the extent observed even if the molecular gas is almost completely confined to a few spiral arms. This is due to both the distance ambiguity, which effectively folds the inner Galaxy emission upon itself when transforming from XY to l-v, and the intracloud and cloud-cloud velocity dispersions, which disperse the emission in that dimension. A very large and very empty interarm hole, such as that shown in **Figure 4**, requires a large area of the inner Galaxy at both kinematic distances to be effectively devoid of molecular gas. Similar very deep interarm holes between the Local arm, Perseus arm (Digel et al. 1996, Heyer & Terebey 1998), and Carina arm (Grabelsky et al. 1987) likewise imply that molecular clouds in the outer Galaxy are almost exclusively confined to the spiral arms.

Regardless of whether the spiral structure is inferred from cloud positions or from modeling, and even if the distance ambiguity can be resolved correctly in all cases, the structure shall be somewhat distorted by both local and large-scale perturbations of the Galactic kinematics. It is as if the inferred spiral pattern is drawn on a rubber sheet that has been stretched and pulled by the Galactic kinematics in ways that are hard to quantify. Some fiducial markers are needed, distinct objects known to be in the spiral arms, for which accurate distances can be determined.

Just such objects are currently being supplied by the ongoing Bar and Spiral Structure Legacy (BeSSeL) Very Long Baseline Array (VLBA) survey of water and methanol masers in high-mass star-forming regions throughout the Galaxy and a similar effort with the Japanese VLBI (very long baseline interferometry) Exploration of Radio Astrometry (VERA) array (Honma et al. 2012, Reid et al. 2014). To date, trigonometric parallaxes and proper motions have been measured for over 100 masers with accuracies of ~10 microarcsec, providing distance uncertainties of ~10% at the distance of the Galactic Center. Nearly all these masers can be unambiguously associated with molecular clouds, which in turn can be associated with well-known spiral features in the CO l-v diagram. In this way, more accurate positions and orientations have been determined for the Outer Spiral Arm (Hachisuka et al. 2009, Sanna et al. 2012), as well as the Perseus (Zhang et al. 2013), Local (Xu et al. 2013), Sagittarius (Wu et al. 2014), Scutum (Sato et al. 2014), and Expanding 3-kpc arms (Sanna et al. 2014). Of course, these studies are also improving our knowledge of the Galactic kinematics, leading to more accurate methods for determining kinematic distances (Reid et al. 2009).

4.5. Vertical Distribution

In contrast to many other aspects of molecular clouds, there has been little controversy regarding their distribution perpendicular to the Galactic plane. Both axisymmetric model fitting and the

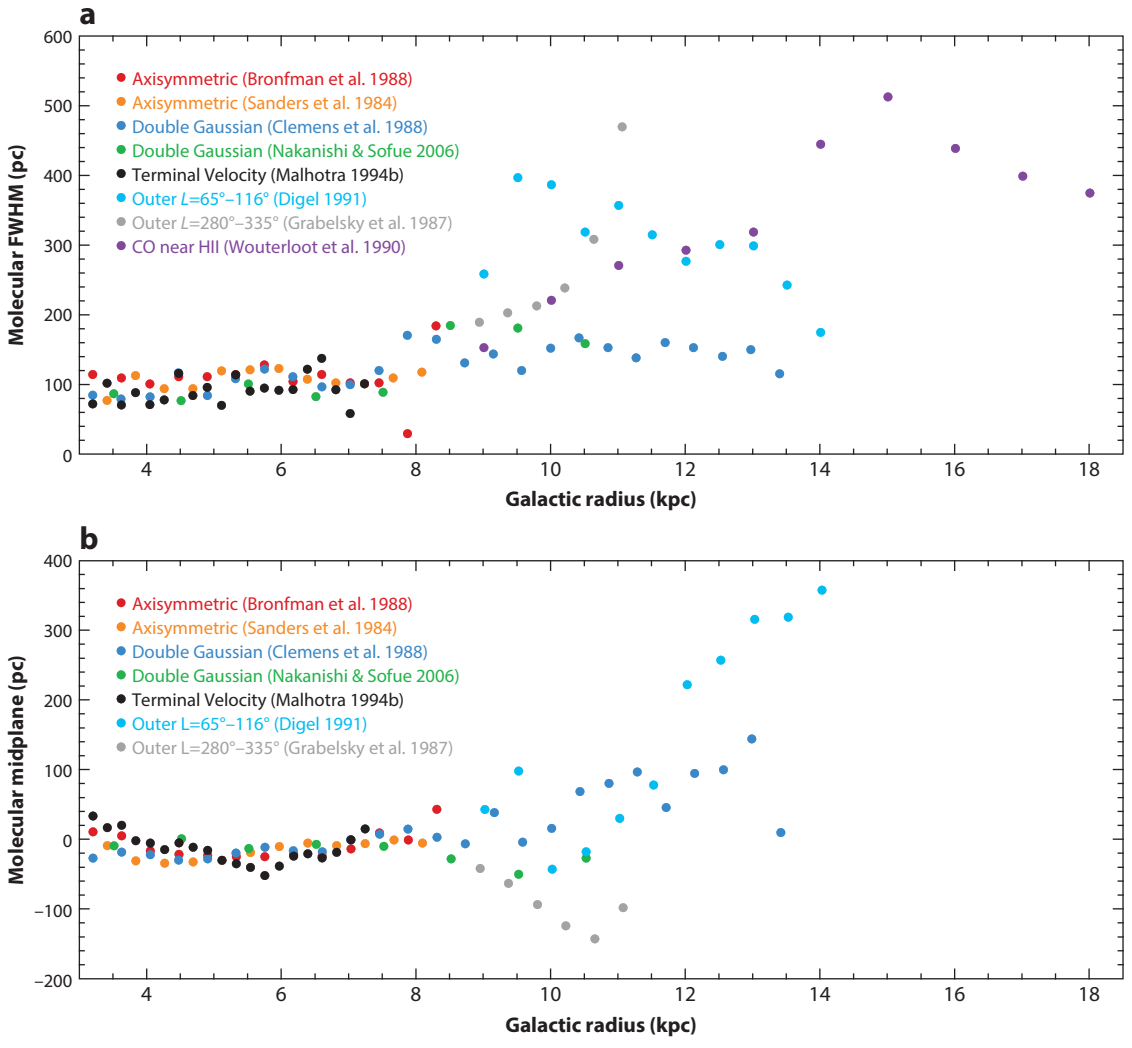

Figure 6

A comparison of measurements of (*a*) the thickness of the molecular gas layer and (*b*) its midplane displacement as functions of Galactic radius.

double Gaussian method have yielded measurements of the average thickness of the molecular gas layer and its deviations from the plane. Although cloud catalogs are not appropriate for such measurements owing to their incompleteness for both small and distant clouds, a third approach is provided by the study of gas near the terminal velocity, where the distance ambiguity reduces to zero (Malhotra 1994b). **Figure 6** shows the radial profiles of the thickness and displacement of the H_2 layer. There is generally good agreement among the three methods within the solar circle, even when applied by different research groups to different CO surveys. All results show a slight rise in the molecular layer thickness, from ∼90 pc (FWHM) at $R = 2$ kpc to ∼120 pc at $R = 8$ kpc and a mean displacement of the midplane below $b = 0$, peaking at ∼30 pc about halfway between the Sun and the Galactic Center.

Examined more closely, however, there is a modest but significant difference in the mean layer thickness as measured at the tangent points relative to that measured by the other methods. Averaging over the Galactic radius range of 2.5–8 kpc, where the most accurate measurements can be made, the axisymmetric model fits of Bronfman et al. (1988) and Sanders et al. (1984) yield mean values for the layer thickness (FWHM) of 102 pc and 103 pc, respectively, and the double Gaussian analysis by Clemens et al. (1988) yields a very similar value, 105 pc. In contrast, the mean value at points along the terminal velocity was measured to be 87 pc by Malhotra (1994b). This difference can be understood as being the result of averaging over nonaxisymmetric corrugations of the plane in all but the tangent point analysis; this averaging widens the mean layer thickness while reducing the mean displacement. For this reason, the most accurate measurements of the molecular layer thickness and displacement are likely provided by the terminal velocity analysis of Malhotra (1994b), even though these measurements sample only two dozen points along the terminal velocity.

Although much of the molecular gas is contained in an approximately Gaussian layer, more sensitive CO observations by Dame & Thaddeus (1994) at several positions near the terminal velocity have provided evidence for a second, faint thick molecular disk about three times as wide as the central layer and comparable with the thickness of the HI layer. Malhotra (1994a) similarly found a population of small, faint CO clouds lying well above the central Gaussian disk in the inner Galaxy. The small number of intermediate-velocity high-latitude molecular clouds discussed by Magnani & Smith (2010) may also belong to the thick disk population. Similar thick molecular disks have been reported in the external spiral galaxies NGC 891 (Garcia-Burillo et al. 1992) and M51 (Pety et al. 2013). Although the origin of this extraplanar H_2 has not been well established, its apparent correlation with spiral arms in both the Galaxy and M51 suggests that it is material that has been expelled from the disk by massive star formation. A number of recent theoretical studies support this possibility (Dobbs et al. 2011).

Even though analysis of the molecular disk beyond the solar circle is aided by the lack of a distance ambiguity, it is hampered by both the warping and flaring of the disk, which requires CO observations over a very large area, and the general paucity of molecular gas in that region, which requires that the observations have high sensitivity. Consequently, the only results to date have been limited to particular longitude ranges (Grabelsky et al. 1987, Clemens et al. 1988, Digel 1991), degraded in resolution to obtain adequate sensitivity (Nakanishi & Sofue 2006) or biased toward HII regions revealed by IRAS (Wouterloot et al. 1990). All these results are shown in **Figure 6**. Contrary to the results within the solar circle, which are almost all based on observations in the first Galactic quadrant, the outer Galaxy results vary widely, mainly owing to the different regions analyzed. It has long been known from 21-cm surveys (Kalberla & Kerp 2009) that the flaring and warping of the outer disk varies strongly with Galactocentric azimuth, and it appears that the molecular disk exhibits a very similar structure (Wouterloot et al. 1990).

4.6. H_2 Mass of the Galaxy

Figure 7 presents the most relevant results on the radial distribution of H_2 mass surface density, Σ_{mol}, in the Galaxy; all results are based on analyses of the only CO survey that fairly uniformly covers the entire Galactic plane (Dame et al. 2001). The surface densities as well as the H_2 masses given below are based on $X_{CO} = 2.0 \times 10^{20}$ cm^{-2} (K km s^{-1})$^{-1}$ and $R_\odot = 8.5$ kpc and do not include the mass of helium mixed with the H_2.

As discussed above, the kinematic distance ambiguity within the solar circle limits us to either axisymmetric model fitting (*black curve* in **Figure 7**) or the double Gaussian approach (*red curve*)

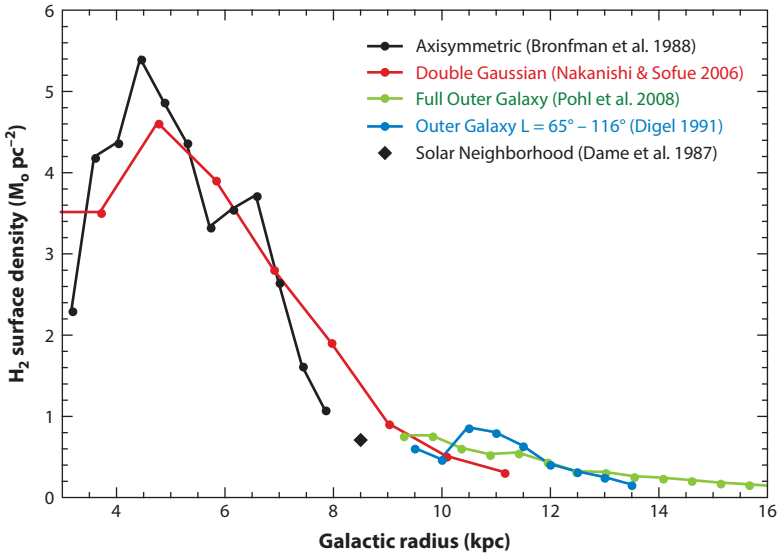

Figure 7

The H_2 mass surface density as a function of Galactic radius. All curves have been scaled to $X_{CO} = 2 \times 10^{20}$ cm^{-2} (K km s^{-1})$^{-1}$, adjusted if necessary to $R_\odot = 8.5$ kpc, and do not include the mass of helium mixed with the H_2.

for determining the distribution and mass of all the molecular gas within the solar circle. It is reassuring that these independent methods yield similar curves and similar H_2 masses within the solar circle ($R = 2$–8.5 kpc): $6.3 \times 10^8\ M_\odot$ (axisymmetric) and $7.5 \times 10^8\ M_\odot$ (double Gaussian). Although the radial distribution derived from the cloud catalog of Roman-Duval et al. (2010) is not directly comparable owing to its incompleteness, its shape is very similar to those shown here.

The H_2 mass at $R_{GAL} < 2$ kpc was estimated by Sanders et al. (1984) to be $1.6 \times 10^8\ M_\odot$ [scaled to $X_{CO} = 2 \times 10^{20}$ cm^{-2} (K km s^{-1})$^{-1}$ and $R_\odot = 8.5$ kpc]. However, evidence from gamma rays (Blitz et al. 1985) and dust emission (Sodroski et al. 1995) strongly suggests that X_{CO} in the Galactic Center is 3–10 times lower than in the disk. The central H_2 mass can therefore be neglected compared with that elsewhere in the disk.

Since the axisymmetric fit parameters are poorly determined near the solar circle owing to the wide latitude coverage required, we omit the axisymmetric result there and instead mark with a black diamond the value within 1 kpc of the Sun as derived by the wide-latitude analysis by Dame et al. (1987).

As we discussed above, the analysis of the molecular gas distribution in the inner Galaxy by Pohl et al. (2008) is complicated, but their analysis beyond the solar circle is simple and straightforward. Adopting a flat rotation curve beyond the solar circle, they derive the H_2 gas distribution there using the entire CfA-U.Chile CO survey. The green curve in **Figure 7** is simply a radial binning of their outer Galaxy gas map and implies a total H_2 mass beyond the solar circle of $2.7 \times 10^8\ M_\odot$. For comparison, we also show an earlier result over a restricted longitude range by Digel (1991) (**Figure 7**, *blue curve*).

For the H_2 mass of the inner Galaxy, we take the mean of the axisymmetric and double Gaussian results and adopt an uncertainty of 30% corresponding to the error on the inner-Galaxy X_{CO} value (Bolatto et al. 2013). The uncertainty on the outer Galaxy mass is larger, owing to both uncertainty

on the rotation curve and X_{CO}. X_{CO} likely increases with radius owing to decreasing metallicity (Balser et al. 2011), but the X_{CO} gradient at present is poorly determined. We therefore consider the outer Galaxy mass to be still uncertain by ~50%. Our best estimate for the Galactic H_2 mass is therefore $(1.0 \pm 0.3) \times 10^9\ M_\odot$.

A few comments are warranted here regarding the so-called dark gas, which is inferred to exist in the ISM by total gas tracers, such as gamma rays and dust, but not revealed by CO and 21-cm surveys (Grenier et al. 2005). The dark gas is generally believed to be H_2 in the lower extinction regions of molecular clouds in which H_2 survives but CO is dissociated (Wolfire et al. 2010). If this is correct, then the classic methods of calibrating the X factor using total gas tracers, such as gamma rays (Strong & Mattox 1996) and dust emission (Dame et al. 2001), already implicitly account for the CO-dark H_2, because any gas not seen in the 21-cm line is assumed to be molecular and used to calibrate X_{CO}. Therefore, the fraction of H_2 that is CO-dark has almost no effect on the curves shown in **Figure 7** nor on our total mass estimate.

5. CLOUD PROPERTIES AND STRUCTURE

> ...the observed motions are all part of a common hierarchy of interstellar turbulent motions.
> —Larson (1981)

The properties of molecular clouds are primarily derived from large surveys of CO emission along the Galactic plane, which span a range in Galactic radius and environmental conditions. The Galactic plane surveys are complemented by high-sensitivity, wide-field imaging studies of CO and the dust component within nearby (<2 kpc) molecular clouds. Although the environment for these targeted clouds is fixed to that of the Solar Neighborhood, the improved sensitivity and high spatial dynamic range of the data reveal the detailed patterns of the gas distribution and kinematics and how these connect to the larger structure of the cloud. In this section, we first summarize the results from the Galactic plane surveys that derive properties integrated over the solid angle of the cloud and then examine the internal structure of molecular regions revealed by wide-field imaging of clouds in the Solar Neighborhood.

5.1. Integrated Properties of Molecular Clouds

Surveys of CO emission along the Galactic plane provide a continuum of information on the molecular gas content of the Milky Way. A common product from these surveys is a catalog of discrete units of CO emission that are representative of molecular clouds. The tabulated cloud properties include centroid positions (l, b, v_{LSR}), angular size, velocity dispersion, and line flux (K km s^{-1} steradian), integrated over the solid angle and velocity extent of the cloud. If distances to the clouds are determined, then the catalogs also list physical size (in parsecs), CO luminosity (K km s^{-1} pc^2), H_2 mass, and cylindrical coordinates, (R_{GAL}, Φ_{GAL}, and z).

The catalogs are constructed on the basis of a definition of a cloud in the position-position-velocity (ppv) space of the spectroscopic observations. This segmentation of the data is especially challenging inside the solar circle owing to velocity crowding of emission near the terminal velocity and blending of emission from unrelated clouds located at the near and far distances along the line of sight. The most frequently applied definition of a cloud is a set of voxels (volume pixels) with brightness temperatures above a user-defined threshold that encloses a contiguous volume in the ppv space. Cloud properties are calculated based on the positional and velocity moments for the set of voxels. Two widely used algorithms that segment ppv data cubes are CLUMPFIND (Williams et al. 1994) and CPROPS (Rosolowsky & Leroy 2006), but the same concept had

been previously developed and applied by Solomon et al. (1987) and Scoville et al. (1987) to the UMSB survey. Variations of these algorithms are described in more recent investigations (Heyer et al. 2001, Brunt et al. 2003, Rathborne et al. 2009, Mottram & Brunt 2010). Other earlier methods include subtracting a smooth background (Dame et al. 1986, Myers et al. 1986) and clipping two-dimensional images of integrated intensity in sections of the Galaxy in which cloud blending is minimal (Dobashi et al. 1996, Yonekura et al. 1997, Kawamura et al. 1998). The algorithm GAUSSCLUMP, described by Stutzki & Guesten (1990), fits a hyper-Gaussian profile to localized emission peaks but has mostly been applied to characterize substructure within molecular clouds rather than to define clouds in the Galactic plane.

For all these catalogs derived from Galactic plane surveys, the intent is to isolate the largest structure that defines the cloud and not the decomposition of the cloud into constituent clumps and cores. Nevertheless, the rigorous application of these algorithms to data frequently identifies distinct objects that are likely part of a larger molecular cloud. This is certainly the case in the catalog by Heyer et al. (2001) but is also evident when comparing the most massive clouds in the Galaxy identified by Dame et al. (1986) with underlying substructure for these fields found with higher angular resolution (Solomon et al. 1987, Issa et al. 1990, Roman-Duval et al. 2010). One can smooth the high-resolution data to connect such distinct objects (Rathborne et al. 2009) but at the risk of blending signal from unrelated clouds. In cases in which the thresholds are high, the derived properties are extrapolated to a lower surface brightness threshold (typically, $T_B = 1$ K) to account for material in the extended cloud envelopes (Scoville et al. 1987, Solomon et al. 1987, Rosolowsky & Leroy 2006).

The cloud catalogs are necessarily affected by both detection and completeness limits that respectively vary with distance and l, b, v_{LSR} position in the survey data. It is straightforward to estimate the detection limit as it depends on the applied cloud definition. The ability to detect and recover a cloud feature with a given set of properties (flux, angular size, velocity dispersion) above the background signal is not as readily determined as the background varies with position and velocity, and the clouds themselves are extended, amorphous structures. Although these algorithms have been extremely useful in compiling the general properties of molecular clouds, these rather simplified definitions of complex structures embedded within a confusing background component are likely responsible for much of the measured variance of cloud attributes.

5.1.1. Molecular cloud mass surface density. The H_2 column density of a molecular cloud averaged over its projected area, commonly called its mass surface density, is a fundamental property of great interest for a number of reasons. It links to the cloud's self-shielding layer responsible for its molecular state, its gravitational potential, its contrast with respect to the surrounding atomic gas substrate, and its contrast to the localized, high-density regions or cores within the cloud. Critical column densities are derived to parameterize instabilities or magnetic fields with respect to self-gravity (Toomre 1964, Mouschovias & Spitzer 1976). The comparison of the measured gas column density of a cloud to these critical column densities evaluates the stability of the cloud with respect to these forces.

For a given value of X_{CO}, the mass surface density of a cloud is directly proportional to the measured mean surface brightness of ^{12}CO emission. We have compiled measurements from the primary ^{12}CO survey catalogs of the Galactic Center (Oka et al. 2001), the molecular ring (Solomon et al. 1987), and the outer Galaxy (Heyer et al. 2001) to express the mean surface brightness, $<W_{CO}> = \int W_{CO} d\Omega / \int d\Omega$. The variation of these quantities averaged within 0.5-kpc bins of Galactocentric radius is shown in **Figure 8**. The rms scatter of surface density values for each survey is rather moderate (20–50%) given the challenges of identifying clouds in the inner Galaxy.

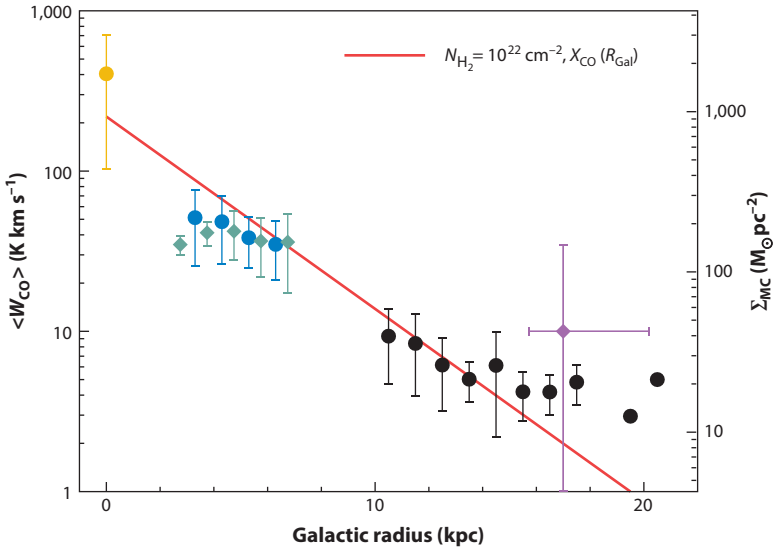

Figure 8

The ^{12}CO surface brightness (*left axis*) and mass surface density (*right axis*) of molecular clouds binned in Galactocentric radius. The error bars reflect the standard deviation of values within each bin; error bars are omitted for bins with only one cloud. The filled circles are derived from ^{12}CO data by Oka et al. (2001, *gold*), Solomon et al. (1987, *blue*), and Heyer et al. (2001, *black*). For these clouds, the corresponding mass surface densities are derived assuming a constant value of $X_{CO} = 2 \times 10^{20}$. The diamonds represent mass surface densities derived from ^{13}CO data from Roman-Duval et al. (2010, *turquoise*) and Brand & Wouterloot (1995, *purple*). For Brand & Wouterloot, we show only the mean radius and mean surface density of their clouds. The horizontal and vertical error bars reflect the range of radii and the estimated dispersion of mass surface density in their sample. The red line shows the variation of $<W_{CO}>$ for constant column density but a radially varying X_{CO} described by Sodroski et al. (1995).

Figure 8 illustrates that the clouds in the outer Galaxy are ~7 times fainter in CO emission than are those in the inner Galaxy and ~60 times fainter than clouds in the Galactic Center. The underluminous nature of clouds in the outer Galaxy was identified by Digel et al. (1990), who attributed it to a reduced CO emissivity per H_2 molecule (larger X_{CO}) in outer Galaxy clouds in response to reduced gas temperatures and metallicities (Narayanan et al. 2012). The red line in **Figure 8** shows the effect of varying X_{CO} in the Galaxy as quantified by Sodroski et al. (1995) for clouds with constant H_2 column density of 1×10^{22} cm^{-2}. Rather than systematic changes in X_{CO}, the reduced surface brightness of outer Galaxy clouds could result from the decreasing mass surface density of clouds in response to environmental conditions, such as the mid-plane pressure or FUV radiation field. If X_{CO} does not change with R_{GAL}, the surface brightness values correspond to cloud surface densities of 1,800 $M_\odot$ pc^{-2} in the Galactic Center, 200 $M_\odot$ pc^{-2} in the molecular ring, and 30 $M_\odot$ pc^{-2} in the outer Galaxy.

Secondary tracers of H_2 column density such as ^{13}CO emission help to resolve this degeneracy. Using data from the BU-FCRAO GRS of ^{13}CO emission, Roman-Duval et al. (2010) calculated cloud surface densities of ~140 $M_\odot$ pc^{-2} that are comparable with the ^{12}CO-derived values. This value is larger than the median surface density of 40 $M_\odot$ pc^{-2} derived by Heyer et al. (2009), who examined ^{13}CO emission within the cloud areas defined by Solomon et al. (1987). However, these cloud areas are generally not filled with detected ^{13}CO emission owing to the effects of reduced excitation and abundance in the cloud envelopes so the corresponding cloud masses are lower

limits. In contrast, Roman-Duval et al. (2010) defined clouds based on detected ^{13}CO emission above a threshold. Although lines of sight with signal near this threshold may also be influenced by subthermal excitation conditions and reduced ^{13}CO abundances, these comprise a small fraction of the cloud area relative to the ^{12}CO-defined surfaces. Wide-field imaging surveys of ^{13}CO emission in the outer Galaxy have only recently been available (Brunt et al. 2015) but have not yet been decomposed into clouds. Brand & Wouterloot (1995) derived column densities from ^{13}CO emission for single or several lines of sight through clouds in the far outer Galaxy. Accounting for the ^{12}C/^{13}C isotopic ratio in this sector of the Galaxy, the median surface density of their sample is 40 $M_\odot$ pc^{-2}. These results suggest that the surface density of outer Galaxy clouds is smaller than clouds residing in the inner Galaxy, but the differences are not as large as implied by $<W_{CO}>$ with a constant value of X_{CO}.

5.1.2. Mean density and temperature of molecular clouds. The gas temperature and density of molecular gas can be constrained by the ratio of line intensities of the low-J rotational transitions of CO. Sakamoto et al. (1997) and, more recently, Yoda et al. (2010) obtained ^{12}CO $J = 2$–1 observations along the Galactic plane to compare with the $J = 1$–0 data from Cohen et al. (1986) and Dame et al. (2001) with the same angular resolution. They classify three types of regions based on the measured ratio, $R = I(2\text{–}1)/I(1\text{–}0)$: very high-ratio gas (VHRG), $R > 1.0$; high-ratio gas (HRG), $0.7 < R < 1.0$; and low-ratio gas (LRG), $R < 0.7$. The median value of R throughout the Galaxy is 0.64 ± 0.05. The physical conditions of each ratio range can be estimated from non-local thermodynamic equilibrium (non-LTE) modeling of CO emission. Using the RADEX code (van der Tak et al. 2007) with $N_{CO}/\delta v \sim 10^{17}$ cm^{-2} (km s^{-1})$^{-1}$, the VHRG gas requires temperatures in excess of 40 K and densities greater than 10^{4-5} cm^{-3}. Such regions are found near localized heating sources such as HII regions and supernovae. The HRG material is less constrained as physical conditions ranging from $(T, n) = (10\,\text{K}, 10^5\,\text{cm}^{-3})$ to $(50\,\text{K}, 250\,\text{cm}^{-3})$ can replicate these ratios. The LRG material is better constrained by the models with (T, n) ranging from (40 K, 100 cm^{-3}) to (10 K, 500 cm^{-3}). These density values are comparable with the mean density of molecular clouds derived from simply dividing the mass by the volume inferred from the projected cloud size. Localized regions with densities much larger than these mean volume densities are directly identified with high-density gas tracers, such as CS, HCN, and N_2H^+ emission lines, or inferred from submillimeter thermal dust continuum emission. However, such regions comprise a small fraction of the cloud mass and volume and do not significantly contribute to the CO luminosity from which the total cloud mass is derived (Battisti & Heyer 2014).

Sakamoto et al. (1997) identified a slight trend of decreasing R values with increasing Galactocentric radius. Because well-resolved clouds exhibit sites with both low and high values of R, Sakamoto et al. (1997) attribute this radial gradient to a radially varying mixing of molecular gas with low and high R values. However, at all locations in the disk, it is the low excitation (low R) material that make the largest contributions to cloud emission.

5.1.3. Molecular cloud mass and size distributions. The measured mass and size of molecular clouds are compiled into distribution functions that characterize the population. The distributions are conventionally expressed as the number of clouds, N, that fall within equal-sized bins, dN/dX, equal-sized logarithmic bins, $dN/d\log X$, or as cumulative functions $dN(X' > X)/dX$. For cloud masses or sizes greater than the completeness limit for a given survey, the equal-sized bin distributions are described by power-law functions, $dN/dX \sim X^{-\alpha_X}$. Here, we explicitly include the negative sign in the expression so α_X is positive-definite. For the logarithmic or cumulative forms, the power-law index is $\alpha_X - 1$.

The most comprehensive views of the cloud mass function are derived from the consolidation of cloud catalogs derived from the different plane surveys. Williams & McKee (1997) fit the compiled masses tabulated by Dame et al. (1986), Solomon et al. (1987), and Scoville et al. (1987) to the function,

$$\frac{\mathrm{d}N}{\mathrm{d}\ln M} = N_{\mathrm{cu}} \left(\frac{M_{\mathrm{u}}}{M} \right)^{-(\alpha_M - 1)} \quad \text{for} \quad M \leq M_{\mathrm{u}} \tag{1}$$

that considers an upper mass limit, M_{u}, to the population. The value N_{cu} is the number of clouds with mass near this high-mass limit. The best-fit values for these parameters are: $\alpha_M - 1 = 0.7$, $N_{\mathrm{cu}} = 10$, and $M_{\mathrm{u}} = 6 \times 10^6\,\mathrm{M}_\odot$ from which two key inferences are made. First, the fact that $N_{\mathrm{cu}} \gg 1$ implies that M_{u} reflects an imposed ceiling to cloud masses that is set by the physical properties of the ISM rather than a statistical artifact. Second, the amount of H_2 mass residing within cataloged clouds is only 40% of the mass inferred from the total observed CO emission—a deficit also recognized by Solomon & Rivolo (1989) following corrections for signal outside of the cloud boundary and the Malmquist bias. Both studies speculate that the missing material resides within small, cold clouds that are too faint to be included in the cloud catalogs.

Rosolowsky (2005) followed this study with additional ^{12}CO data from the catalogs of outer Galaxy clouds compiled by Heyer et al. (2001) and Brunt et al. (2003) as well as resolved molecular complexes in Local Group galaxies. Accounting for both measurement errors and sample variance, they calculated values of α_M, N_{cu}, and M_{u} similar to those determined by Williams & McKee (1997) in the inner Galaxy surveys but derive steeper power-law indices ($\alpha_M - 1 > 1$) for molecular clouds in both the outer Galaxy and the Local Group. For the outer Galaxy sample, the steeper power law may result from the higher spatial resolution obtained there, which allows clumps and filaments of larger clouds to be identified as distinct objects, thus enhancing the population in smaller mass bins. For M33 and the Magellanic clouds, the steeper slopes may indicate that the different dynamical and interstellar conditions relative to those in the inner Milky Way may limit the production of massive GMCs there.

The distribution of cloud size, L, is not as frequently derived from the CO surveys yet can offer additional insight to the molecular cloud population. Like the mass spectrum, the size distribution is expressed in differential form, $\mathrm{d}N/\mathrm{d}L \sim L^{-\alpha_L}$. Using the data from Solomon et al. (1987), Elmegreen & Falgarone (1996) derived the index $\alpha_L = 3.4$. The larger-sized catalogs from the FCRAO surveys result in similar values: 3.3 ± 0.1 for the outer Galaxy (Heyer et al. 2001) and 3.9 ± 0.7 for the molecular ring on the basis of ^{13}CO $J = 1$–0 emission (Roman-Duval et al. 2010).

In the context of the cloud description of the molecular ISM, these values of α_M and α_L provide a basic characterization of the cloud population. The majority of clouds are small with low masses. Most of the molecular mass in the Milky Way resides within clouds with masses greater than $10^5\,\mathrm{M}_\odot$ and there is an upper mass limit of $\sim 5 \times 10^6\,\mathrm{M}_\odot$.

Elmegreen & Falgarone (1996) and Elmegreen (2002) offer an alternative interpretation of the cloud mass and size distributions in which the identified clouds are the peaks of a pervasive fractal molecular medium with dimension D_{f}. Structures extracted from such a medium, using the same threshold methodology as that which observers apply to CO surveys, follow a mass-size relationship such that $M \sim L^{D_{\mathrm{f}}}$ and are distributed in mass and size similar to the observations. Although this view does not exclude the concept of discrete cloud structures, it does emphasize that more extended and unseen structure is present in the neutral ISM in the form of dark gas and atomic gas. Molecular clouds are not isolated objects but are part of the multiphase ISM. The structures measured with CO emission are simply volumes in which CO is sufficiently self-shielded from dissociating UV radiation.

5.1.4. Larson scaling relationships between integrated properties. For over thirty years, the three Larson (1981) scaling relationships have provided the primary observational constraints on the dynamics of molecular clouds. Using data from the literature then available, Larson established a power-law scaling between velocity dispersion, σ_v, and cloud size, L, with an index of 0.38; an inverse relationship between the mean density of the cloud, $<n_{MC}>$, and L, and the relationship $2GM_{MC}/\sigma_v^2 L \sim 1$. These scaling relationships are conventionally interpreted in sequence to imply: (*a*) molecular clouds are turbulent structures; (*b*) the mass surface density does not significantly vary among molecular clouds; and (*c*) an equipartition exists between gravitational and kinetic energy densities. The three relationships are not independent—the validity of any two of the expressions algebraically implies the third. This coupling is encapsulated in the singular expression that equates the virial mass to the mass of the cloud,

$$\sigma_v = (\pi G/5)^{1/2} R_{MC}^{1/2} \Sigma_{MC}^{1/2}, \quad (2)$$

where $R_{MC} = L/2$ is the cloud radius. This expression implies a scaling exponent of 1/2 for the line width–size relationship for constant mass surface density, rather than the value ~0.4 originally derived by Larson (1981).

The CO Galactic plane surveys have played an important role in the development and refinement of these scaling relationships as these provide a homogeneous set of data with large samples of molecular clouds that span a broad range of conditions in the Galaxy. Cloud properties tabulated by Dame et al. (1986), Solomon et al. (1987), and Scoville et al. (1987) all imply a virial parameter, $\alpha_{vir} = M_{vir}/M_{MC} \sim 1$, indicative of gravitationally bound clouds in equilibrium. Sodroski (1991) noted that the outer Galaxy clouds appear to have virial masses much larger than CO derived masses. A subsequent study by Falgarone et al. (1992) and ^{13}CO $J = 1$–0 surveys in the Cygnus (Dobashi et al. 1996) and Cepheus (Yonekura et al. 1997) sectors of the Galactic plane also found virial masses much larger than CO-derived masses for clouds less than ~1,000 $M_\odot$. Heyer et al. (2001) confirmed these findings from ^{12}CO-derived clouds in the outer Galaxy. The absence of low-mass, gravitationally bound clouds is imposed by selection effects from the cloud identification method that requires a minimum number of spectral channels and pixels above an antenna temperature threshold. Lower-mass clouds or clumps could be present, as found in the Solar Neighborhood, but are excluded from the derived catalogs that are based on the cloud definition. Those objects (clumps or clouds) with $\alpha_{vir} \gg 1$ that are compiled within the cloud catalogs are either bound by external pressure (Bertoldi & McKee 1992) or short-lived in these configurations with respect to their dynamical timescales of (5–10) $\times$ 10^6 years. Alternatively, one could rectify the seemingly unbound clouds by adopting a larger value for X_{CO} in the outer Galaxy as proposed by Sodroski (1991). But applying this larger X_{CO} value to the massive clouds for which $\alpha_{vir} \sim 1$ using the standard value would imply that these volumes should be in a state of global, gravitational collapse for which there is no current evidence.

Larson (1981) constructed the line width–size relationship using gas tracers with varying excitation requirements that sample different size scales. The use of multiple line tracers extended the dynamic range of size scales, which enabled the trend with velocity dispersion to be recognized. Since this study, many types of line width–size relationships have emerged from the observational record. Goodman et al. (1998) classified four types of relationships based on how these are constructed: Type 1, multitracer, multicloud; Type 2, single-tracer, multicloud; Type 3, multitracer, single cloud; and Type 4, single tracer, single cloud. The line width–size relationship identified by Larson (1981) is Type 1. The correlation between cloud velocity dispersion and size constructed from the Galactic plane surveys is Type 2.

The variation of ^{12}CO velocity dispersion with cloud radius, R_{MC}, for molecular clouds located in the Galactic Center (*gold*), molecular ring (*blue* and *red*), and outer Galaxy (*black*) is shown in

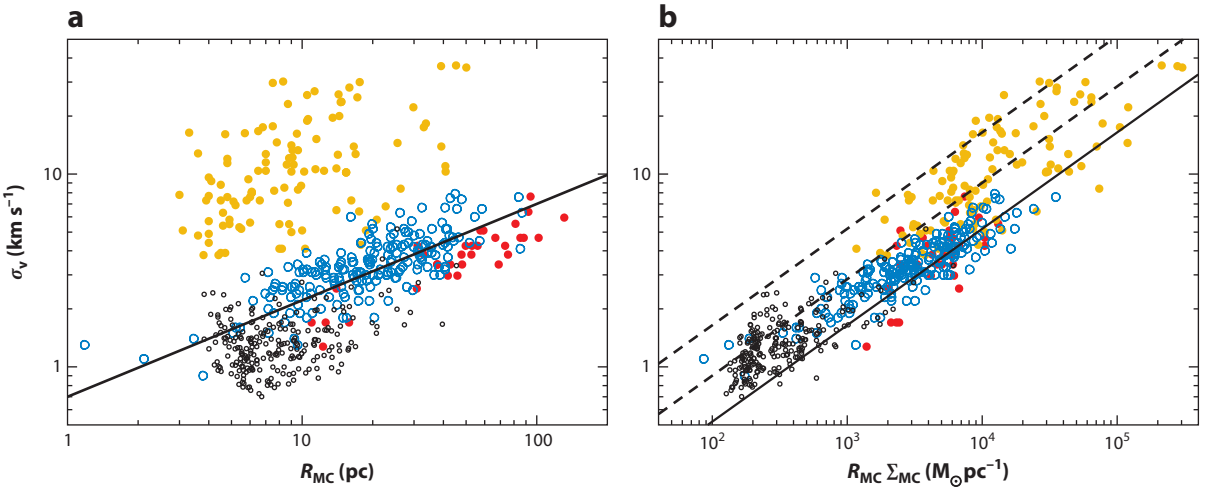

Figure 9

(*a*) The variation of cloud velocity dispersion with size from the molecular cloud catalogs by Dame et al. (1986, *red*), Solomon et al. (1987, *blue*), Oka et al. (2001, *gold*), and Heyer et al. (2001, *black*). The outer Galaxy cloud sample is restricted to clouds with $v_{LSR} < -25$ km s^{-1} to limit kinematic distance uncertainties and mass >2,500 $M_\odot$, where the catalog is complete. The solid line shows the best-fit to the Solomon et al. (1987) points. (*b*) The variation of cloud velocity dispersion with the product of size and mass surface density. The solid line corresponds to Equation 2 and the two dotted lines show loci for $\alpha_{vir} = 3$ (*lower*) and 10 (*upper*).

Figure 9*a*. The data from Solomon et al. (1987) show the strongest correlation. The Galactic Center clouds exhibit a relationship with larger scatter and velocity dispersions approximately five times larger than the value for disk molecular clouds of the same size. Shetty et al. (2012) find similar results using high-density gas tracers of Galactic Center clouds. In contrast, a line width–size relationship is not readily evident for clouds in the outer Galaxy sample as there is limited dynamic range of cloud sizes and a large scatter of σ_v values. For the same reasons, the correlation is also absent in the catalogs of Dobashi et al. (1996) and Yonekura et al. (1997). Moreover, the velocity dispersions of outer Galaxy clouds are well displaced below the scaling relationship defined by the inner Galaxy molecular clouds. Falgarone et al. (2009) extended the line width–size relationship to small clouds and cloud clumps but noted the increased scatter of line widths for sizes less than 1 pc.

It appears that the line width–size relationship breaks down when including clouds located within these extreme locations of the Galaxy. However, a key result in Larson's scaling relationships is a constant surface density for all clouds. As **Figure 8** illustrates, there are variations of the mass surface density within each radial bin as well as a systematic fall-off with increasing R_{GAL} for a constant value of X_{CO}. **Figure 9*b*** shows the variation of σ_v with the product $R_{MC}\,\Sigma_{MC}$. Clouds within the Galactic disk follow the scaling relationship implied by Equation 2. It should be noted that the observed correlation arises, in part, from the dependence of CO column density on the integrated intensity for each line of sight, which includes the CO profile line width, and the dependence of the integrated velocity dispersion on cloud size. Using dust emission from *Herschel* as an independent measure of column density, Arzoumanian et al. (2013) verify that σ_v scales as $\sim\Sigma_{MC}^{1/2}$ as implied by **Figure 9**.

Clouds within the Galactic disk have virial ratios between 1 and 3 that are consistent with being gravitationally bound given the systematic errors of recovering cloud properties. A similar

correlation between velocity dispersion and $R_{MC}\Sigma_{MC}$ is found in the properties of clouds derived from ^{13}CO (Heyer et al. 2009) and molecular clouds in nearby galaxies (Bolatto et al. 2008, Leroy et al. 2014). Clouds in the outer Galaxy with masses below the completeness limit (not shown in **Figure 9**) exhibit higher virial ratios and a large scatter of velocity dispersions with respect to $R_{MC}\Sigma_{MC}$ (Heyer et al. 2001, Leroy et al. 2015). The set of Galactic Center cloud points are parallel to Equation 2 but are vertically displaced, corresponding to α_{vir} between 3 and 10. If the true X_{CO} value for the Galactic Center is less than the Galactic average, as implied by IR (Sodroski et al. 1995) and gamma-ray (Blitz et al. 1985) measures of H_2 column density, then these points become even further removed from gravitational equilibrium.

The $\sigma_v - R_{MC}\Sigma_{MC}$ relationship has been broadly interpreted. Ballesteros-Paredes et al. (2011) interpret the displacement and correlation of $\sigma_v/R_{MC}^{1/2}$ with $\Sigma_{MC}^{1/2}$ as collapsing clouds so that σ_v reflects infalling motion of gas toward a local potential minimum rather than turbulent flows. Heyer et al. (2009) describe the values of Σ_{MC} as lower limits owing to the effects of ^{13}CO excitation and abundance such that these clouds are in approximate equipartition between gravity and kinetic energy. To determine whether these are collapsing objects or clouds in approximate virial equilibrium requires more precise measures of mass surface density as may be provided by dust or more detailed examination of velocity structure within clouds that can distinguish collapsing motions from turbulent flows. Clouds with $\alpha_{vir} \gg 1$ have velocity dispersions in excess of Equation 2 but may still follow a line width–size relationship that is independent of Σ_{MC}. Such clouds must be short-lived or confined by external pressure (McKee et al. 2010, Field et al. 2011, Hennebelle & Falgarone 2012).

5.2. Cloud Structure and Kinematics

Over the past 15 years, there has been significant progress in measuring and quantifying the gas structure and kinematics within clouds from observations of CO and dust extinction and emission. This progress is well matched to both analytical and computational studies, which examine the effects of gravity, magnetohydrodynamic turbulence, and feedback processes from newborn stars on cloud structure.

A key requirement to investigate cloud structure is coverage with high spatial dynamic range ($>10^4$), in which spatial dynamic range is defined as the ratio of the solid angle of covered area to the solid angle of the resolution element. Such high spatial dynamic range data are realized with IR extinction maps derived from IR all-sky surveys, such as 2MASS; far-IR dust emission from space platforms (IRAS, *Spitzer*, *Herschel*, *Planck*); and wide-field, spectroscopic imaging of ^{12}CO and ^{13}CO line emission with heterodyne, focal plane arrays on single-dish telescopes (Narayanan et al. 2008, Dent et al. 2009, Buckle et al. 2010, Shimajiri et al. 2011, Schneider et al. 2011, Carlhoff et al. 2013). **Figure 10** illustrates the intricate gas distribution and velocity structure of molecular clouds that is revealed by high spatial dynamic range imaging of CO emission from nearby clouds. Typically, such imagery comes from targeted observational programs toward nearby molecular clouds, such as Orion, Perseus, and Taurus, and to a lesser extent, relatively nearby (<2 kpc) clouds extracted from the Galactic plane surveys.

5.2.1. Column density distribution within molecular clouds. The column density distribution within molecular clouds is derived from observations of the dust component and molecular line observations. The IR data are sensitive to a broad range of hydrogen column densities—0.5–30 A_V for dust extinction and 0.1–100 A_V for far-IR/submillimeter dust emission. Both tracers include dust within atomic, dark, and H_2 gas, as well as high volume density cores within clouds. CO-derived column densities are generally limited to the equivalent visual extinction range of

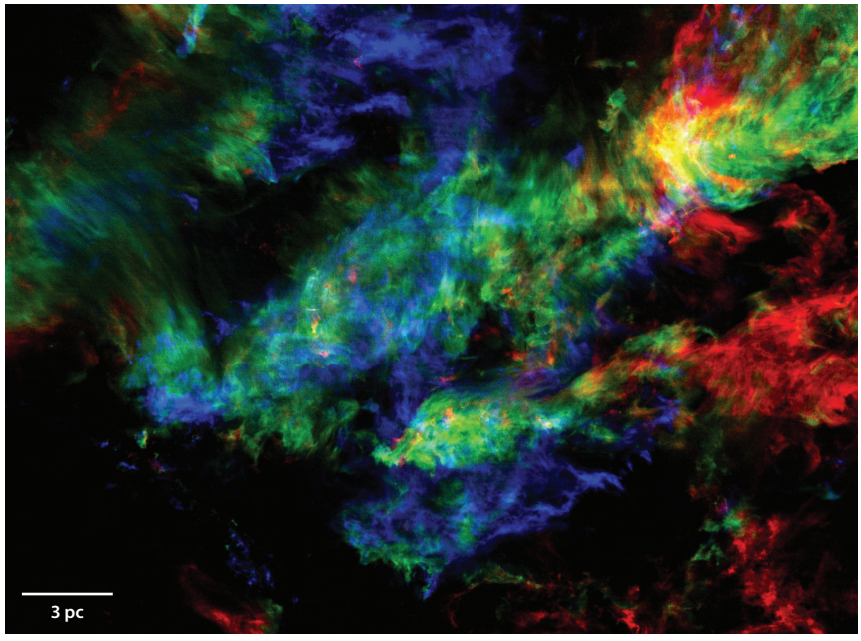

Figure 10

An image of ^{12}CO $J = 1$–0 emission from the Taurus molecular cloud integrated over v_{LSR} intervals 0–5 km s^{-1} (*blue*), 5–7.5 km s^{-1} (*green*), and 7.5–12 km s^{-1} (*red*), illustrating the intricate surface brightness distribution and complex velocity field of the Taurus cloud. The data are from Narayanan et al. (2008). Adapted from figure 12 of Goldsmith et al. (2008) and reproduced with permission from AAS.

2–7 magnitudes (J.E. Pineda et al. 2008, J.L. Pineda et al. 2010, Ripple et al. 2013)—bounded at the low end by rapidly decreasing CO abundances relative to H_2 and low excitation and at the high end by high opacity and decreasing abundance as CO depletes onto cold grain surfaces.

The earliest CO maps of molecular clouds with even moderate spatial resolutions revealed the complex distribution of material (Kutner et al. 1977, Blair et al. 1978, Blitz & Thaddeus 1980, Schloerb & Snell 1984). These maps show localized peaks of molecular line emission or extinction with sizes 10–30% the size of the larger cloud. More sensitive observations identify a low surface brightness component to most clouds in which the CO is subthermally excited owing to low volume densities (Carpenter et al. 1995, Goldsmith et al. 2008). With increasing angular resolution and sensitivity, hierarchical structure becomes more evident as localized, high-density peaks are found within larger clump structures, which themselves reside within the larger molecular cloud complex (Scalo 1985, Rosolowsky et al. 2008). The cloud complexes may be gravitationally bound to even larger supercomplexes labeled giant molecular associations (Vogel et al. 1988). Giant molecular associations are identified in CO imaging surveys of nearby, face-on galaxies but are not readily recognized in the Milky Way owing to ambiguity of linking discrete features together along the Galactic plane. The dense, protostellar cores of molecular clouds from which stars condense are isolated in maps of high gas density tracers and lie at the bottom of this hierarchy. Here we use the conventional nomenclature to distinguish clumps from cores (Goldsmith 1987, McKee & Ostriker 2007). Clumps are intermediate-sized substructures with larger column and volume densities than the parent molecular cloud. Cores are localized, high volume density features that reside within clumps.

The cloud-finding algorithms discussed in Section 5.1 were initially developed to encapsulate this hierarchical structure within the maps of molecular line emission (Stutzki & Guesten 1990, Williams et al. 1994, Rosolowsky & Leroy 2006). These algorithms have been subsequently adapted and applied to two-dimensional data of cloud column densities provided by dust extinction and dust emission maps (Motte et al. 2003, Román-Zúñiga et al. 2009). Like the molecular clouds, the results of such clump-finding analyses are ultimately limited by the definition of the clump in the ppv domain and the intrinsic error connected to the transformation of density, velocity, and temperature fields into the measured set of spectra or continuum emission from which the clumps are defined. Beaumont et al. (2013) have examined these errors by computing synthetic, molecular line spectral data cubes from the density, temperature, and velocity fields produced from computational simulations of interstellar turbulence while also accounting for the photochemistry of H_2 and CO. They find that the clump or object properties derived from ^{13}CO line emission are more reliable than those using the optically thick ^{12}CO line. The errors of the derived properties vary within the cloud depending on emission filling factor but range from 40% for the parameters σ_v, size, and mass and 100% for the virial parameter, $\alpha_{\rm vir}$. They also find that the Larson scaling relationships should be evident in the clumps extracted from the synthetic data cubes. However, when applied to real data, the Larson relationships are not so readily produced by these analyses, as the dynamic range of clump size is typically less than 10 and the scatter of properties is large (Carr 1987, Stutzki & Guesten 1990, Simon et al. 2001, Schneider & Brooks 2004, Wong et al. 2011). Some of this scatter may originate from the superposition of features along the line of sight that are merged into a single object (Ostriker et al. 2001).

The primary observed metric to emerge from the clump-finding analyses is the mass distribution that is directly analogous to the cloud mass spectrum discussed in Section 5.1.3. The measured clump mass spectrum index ranges from 1.6–1.8, which is similar to that derived for molecular clouds and implies that most of the clump mass of a cloud resides within the largest clumps (Kramer et al. 1998). Elmegreen & Falgarone (1996) and Stutzki et al. (1998) cite this similarity as further evidence for a fractal distribution of the ISM as the clumps represent yet another level in the ISM hierarchy. The clump mass distributions within clouds are distinguished from the mass distribution of protostellar cores that follow a log-normal function with a peak at a characteristic mass of $\sim 0.6 - 1\,M_\odot$ (Motte et al. 1998, Testi & Sargent 1998, Alves et al. 2007, André et al. 2010, Könyves et al. 2010) yet are similar in shape to the stellar initial mass function (Salpeter 1955, Miller & Scalo 1979, Chabrier 2003).

The density structure of a molecular cloud is further discerned from one-point and two-point statistics, which consider the available cloud data as a continuum of information rather than a collection of discrete objects or clumps. With its exquisite sensitivity to H_2 column density over large areas, IR-derived dust extinction and emission imagery of molecular clouds have been used to compute the column density probability distribution function (PDF); they have also been used to compute the dense gas mass fraction (DGMF), which reflects the fractional mass of the molecular cloud as a function of column density. These simple, single-point statistics are effective tools to distinguish different dynamical components within molecular clouds (Kainulainen et al. 2009; Lada et al. 2010, 2012; Schneider et al. 2011, 2015; Kainulainen & Tan 2013). Within the low column density regime, the column density PDFs follow log-normal functions that are the product of supersonic turbulent flows (Passot & Vázquez-Semadeni 1998, Ostriker et al. 2001). In the high column density regime of star-forming clouds, the IR-derived PDFs diverge from this log-normal shape and follow a distinct power-law form (Kainulainen et al. 2009, Froebrich & Rowles 2010, Schneider et al. 2015). After accounting for contamination by foreground dust components, the break from the log-normal shape of the PDF occurs at $A_V \sim 4$–5 mag (Schneider et al. 2014). The high column density tail is not evident in PDFs derived from CO observations as both ^{13}CO

and ^{12}CO do not effectively probe the high-density regime of molecular clouds (Goodman et al. 2009).

The high-density tails of the column density PDF are clues to the processes responsible for seeding dense, protostellar cores from which newborn stars condense. Schneider et al. (2015) propose that the power-law tail of the column density PDF results from condensations that emerge from gravitational collapse on all scales—clouds to filaments and filaments to high-density cores. Kainulainen et al. (2013) used numerical simulations to link the slope of the DGMF tail to the amount of power resident within the longitudinal (compressive) component of the velocity field. Low star-forming efficiencies are found in simulations with incompressible turbulence as these generate fewer high-density condensations. Simulations with compressive driving generate larger dense gas fractions that support the formation of massive stars and stellar clusters.

Although the column density PDFs offer valuable information on cloud structure, it is the shape and width of the volume density PDFs of molecular clouds that are used in analytical theories of star formation to predict star-formation rates and the mass distribution of newborn stars (Padoan & Nordlund 2002, Krumholz & McKee 2005, Hennebelle & Chabrier 2008). The width of the volume density PDF, $\sigma_{\rho/\rho_\circ}$, is related to the Mach number, M, of the cloud as $\sigma^2_{\rho/\rho_\circ} = b^2 M^2$. Given the complexity of molecular clouds and the nonlinear transformation of density and velocity fields to the ppv domain of molecular line observations, it is improbable that one could reliably invert a set of measurements to recover the volume density field of the cloud from which the PDF could be derived. However, Brunt et al. (2010a,b) demonstrate that the variance and shape of the volume density PDF can be recovered from the projected column density field in the limit of an isotropic density field. Applying this analysis to the ^{13}CO $J = 1$–0 emission and extinction maps of the Taurus molecular cloud, Brunt (2010) calibrated the coefficient, $b = 0.48^{0.15}_{-0.11}$, to the density variance–Mach number relationship, which agrees with results of numerical experiments.

5.2.2. Cloud velocity structure. The most unique and powerful attribute of high spectral resolution imaging of molecular line emission is the kinematic information conveyed by the spatial variations of the line profiles, which provide a map of the line of sight motions within a molecular cloud. Molecular transitions with different excitation requirements probe different volumes and density regimes within clouds. Wide-field imaging of the low-J rotational transitions of CO covers much of the strongly self-shielded volumes of molecular clouds and the largest range of spatial scales, and therefore, offers the richest bounty of velocity information. The primary challenge in leveraging this information is accounting for variations of line opacity, excitation, and molecular abundances along the line of sight.

For kinematically well-isolated clouds, the one-dimensional velocity dispersion of a CO spectrum for a given position on the sky, $\sigma_{v,p}$, ranges from 1–5 km s^{-1} depending on the cloud size and spatial resolution of the measurement. For a mostly optically thin tracer like the ^{13}CO $J = 1$–0 line, the corresponding full widths of the line profiles reflect the range of projected velocities through the cloud. This range is much larger than the sound speed of gas at typical CO cloud temperatures of 10–20 K but is comparable with the Alfvén velocity of 2.5 km s^{-1} for clouds with a magnetic field strength of 30 μ gauss and mean density of 250 cm^{-3} (Crutcher 1999, Crutcher et al. 2010).

An early model of line emission from the Orion molecular cloud attributed the large widths of molecular line profiles to global collapse of the cloud (Goldreich & Kwan 1974). Zuckerman & Palmer (1974) countered that most molecular clouds in the Milky Way could not be in a state of global collapse as this would imply a star-formation rate much larger than the measured value of $1 - 3\,M_\odot\,\mathrm{year}^{-1}$. More recently, the global collapse of clouds has been reconsidered on the

basis of evidence for rapid star formation (Elmegreen 2000, Hartmann et al. 2001) and numerical simulations of cloud formation (Vázquez-Semadeni et al. 2007). These authors propose that the velocity dispersion of molecular clouds reflects infalling motions rather than the equipartition of gravity and kinetic energy. To address the star-formation rate conundrum raised by globally collapsing clouds, they suggest that the protostellar winds and photoionization produced by the first generation of stars formed by rapid collapse quench much of the subsequent star formation. In this scenario, only a small fraction of the cloud mass is converted into stars.

The supersonic motions in molecular clouds are most frequently linked to turbulent flows (Larson 1981). The Reynolds number, $R_e = Lv/\eta_{\rm kin}$, where L is the spatial size scale, v is the mean flow velocity, and $\eta_{\rm kin}$ is the kinematic viscosity, expresses the ratio of inertial forces to viscous forces of a gas or fluid. In laboratory experiments, turbulent phenomena emerge when $R_e > 10^3$. For viscosity due to molecular collisions, the Reynolds number in molecular clouds is $>10^8$, so turbulent motions should prevail within these domains.

The scaling of velocity dispersion or velocity differences with spatial scale is an informative metric for any velocity field—turbulent or otherwise. Such metrics are encapsulated in the power spectrum or more generally, the structure function,

$$S_p(\tau) = <|v(r) - v(r+\tau)|^p>, \quad (3)$$

where $v(r)$ is the velocity at position, r, τ is the spatial displacement from r, p is the order, and the difference between the velocities is averaged over the volume of the field. For a limited range of spatial scales corresponding to the inertial range, over which energy cascades between different scales without dissipation, $S_p(\tau)$ may follow a power law, such that $S_p(\tau) \sim \delta {\rm v}^p \sim \tau^{\zeta_p}$. Differential information resides within structure functions over a sequence of p values. The higher orders of the structure function are sensitive to non-Gaussian spatial-temporal velocity fluctuations that are the prime signature to turbulence intermittency caused by the highly localized dissipation or injection of energy (Hennebelle & Falgarone 2012). The sequence of power-law indices, ζ (p), is modeled by phenomenological theories of turbulence (Kolmogorov 1941, She & Leveque 1994, Boldyrev 2002).

The spatial statistics of molecular cloud velocity fields, as derived from molecular spectroscopy, have played a key role in advancing our knowledge of interstellar cloud dynamics. The primary metric has been the line width–size relationship within a cloud as it relates to the velocity structure function or power spectrum. Here, we refer to the first-order expression of the line width–size relationship as $\delta v = v_\circ \tau^\gamma$, although this may be derived from a higher-order measure, such that $\gamma_p = \zeta_p/p$.

Methods have been developed to derive the functional form of the velocity power spectrum or structure function from observations. These include the spatial statistics of velocity centroid maps (Scalo 1984, Kleiner & Dickman 1985, Miesch & Bally 1994, Stutzki et al. 1998, Esquivel & Lazarian 2005, Hily-Blant et al. 2008), principal component analysis (PCA) of the cloud line profiles (Heyer & Schloerb 1997, Brunt & Heyer 2002a, Brunt & Heyer 2013), and Fourier analysis of two-dimensional images integrated over both narrow and wide velocity intervals (velocity channel analysis) (Lazarian & Pogosyan 2000). **Figure 11*a*** shows the velocity structure function derived from ^{12}CO and ^{13}CO $J = 1$–0 emission from the Taurus cloud using PCA. Each of these methods have been formally connected to the spatial statistics of the three-dimensional velocity field and verified with velocity and density fields from numerical simulations. For velocity centroid analyses, several orders of the structure function can be derived given sufficient spatial dynamic range and prudent attention to the effects of random noise on the centroid velocity and its propagation to high-order velocity differences (Hily-Blant et al. 2008). All these methods correspond to

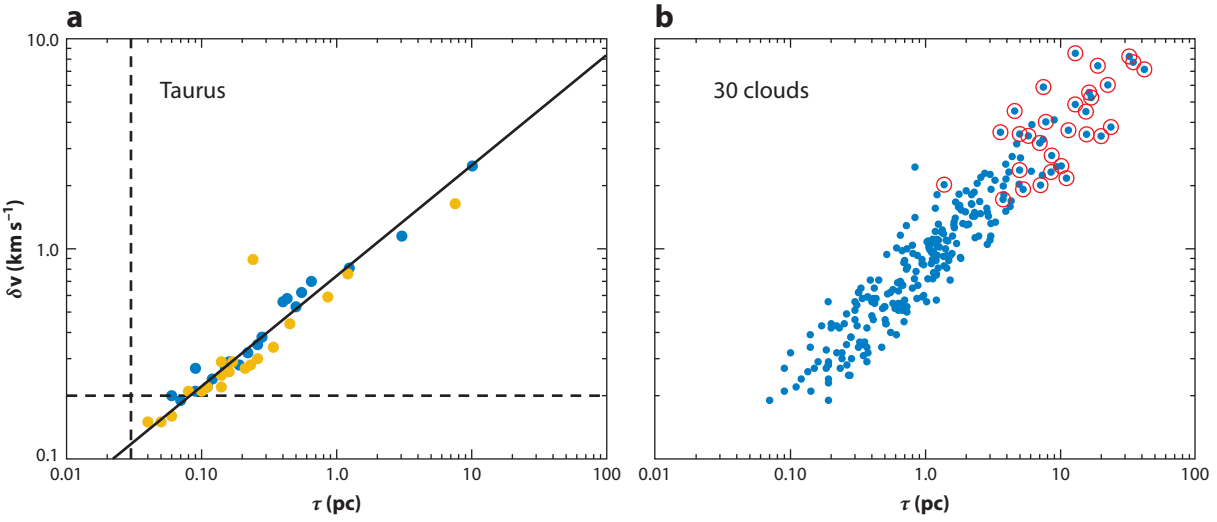

Figure 11

(*a*) The velocity structure function for the Taurus molecular cloud derived using principal component analysis (PCA) with ^{12}CO (*blue*) and ^{13}CO (*gold*) data from Narayanan et al. (2008). The solid line shows the power-law fit to all points. The horizontal and vertical dashed lines mark the spectral and spatial resolutions of the data, respectively. (*b*) Overlaid velocity structure functions for 30 clouds in the Solar Neighborhood and the Perseus arm derived from ^{12}CO emission using PCA (*blue*). Data are from Heyer & Brunt (2004), Ridge et al. (2006), Narayanan et al. (2008), and Ripple et al. (2013). The points circumscribed by red circles mark the structure function evaluated at the largest derived scale and define a Type 2 line width–size relationship that emerges from the alignment of the individual cloud structure functions.

Type 4 velocity dispersion relationships that are constructed from a single tracer of gas velocities within a single cloud (Goodman et al. 1998).

To date, the most broadly applied studies are those by Miesch & Bally (1994), and the PCA results of Brunt & Heyer (2002b), Brunt (2003), Heyer & Brunt (2004), and Roman-Duval et al. (2011). Miesch & Bally (1994) used maps of ^{13}CO emission from 12 nearby clouds composed of 10^3 to 10^4 pixels to derive the second-order structure functions from centroid velocity maps. They found second-order scaling exponents, ζ_2, ranging from 0.4 to 1.4 with a mean value of 0.86 $\pm$ 0.3, corresponding to an equivalent first-order structure function exponent, γ_2 of 0.43 $\pm$ 0.15. Both Brunt (2003) and Heyer & Brunt (2004) applied PCA to a set of spectroscopic data cubes of ^{12}CO $J = 1$–0 emission from molecular clouds in the Solar Neighborhood and the Perseus arm to recover the first-order, velocity structure function (see **Figure 11*b***). The mean and standard deviation of the power-law indices and the scaling coefficients are 0.49 $\pm$ 0.15 and 0.9 $\pm$ 0.2 km s^{-1} pc$^{-1/2}$, respectively. Roman-Duval et al. (2011) extended this work to ^{13}CO $J = 1$–0 emission from 367 molecular clouds in the inner Galaxy to derive a similar, mean scaling exponent, 0.5 $\pm$ 0.3. The results of these different analyses for large numbers of targets, as well as more limited studies with other methods, certify a mean scaling exponent of ~0.5, which points toward compressible turbulence in molecular clouds.

The convergent values of both the power-law index and amplitude that describe the individual velocity structure functions of molecular clouds with comparable mass surface densities attest to the universality of turbulence. **Figure 11*b*** illustrates the alignment of velocity structure functions for 30 clouds in the Solar Neighborhood and the Perseus spiral arm. This near-invariance of velocity structure functions connects the Goodman et al. (1998) Type 4 relationships to the

Type 2 (single tracer, multiple cloud) integrated line width–size relationship discussed in Section 5.1 and illustrated in **Figure 9**. The global velocity dispersion of a molecular cloud, σ_v, is simply the structure function evaluated at the size scale of the cloud, $2R_{\rm MC}$. If the individual structure functions of molecular clouds are aligned, then the endpoints of each structure function are also necessarily aligned, as shown in **Figure 11**. Heyer & Brunt (2004) used the measured scatter of the Type 2 relationship identified by Solomon et al. (1987) to constrain the fractional variations of the power index and scaling coefficient to be less than 20%. The subsequent study by Heyer et al. (2009) and further illustrated in **Figure 9*b*** shows that the value, $\sigma_v / R_{\rm MC}^{1/2}$, depends on surface density as $\Sigma_{\rm MC}^{1/2}$ for gravitationally bound clouds. The Type 2 relationships emerge from the more fundamental Type 4 relationships in the limit of universal velocity structure functions for a set of clouds with comparable mass surface density. The limited range of the scaling coefficient, $v_\circ$, for clouds in the Galactic disk suggests a common formation mechanism of molecular clouds from the atomic medium and a small contribution of internal feedback processes by newborn stars relative to some external source of energy (Larson 1981). This latter implication is further emphasized by Heyer & Brunt (2004) and Heyer et al. (2006) as their samples include molecular clouds with massive star formation and others with little star-formation activity.

Although turbulence describes the random velocity component of cloud motions, the rotation or spin of the cloud, if present, represents large-scale, systematic motions. Observationally, these rotational motions are inferred from the ordered shift of velocity centroids of molecular line emission. The investigation by Koda et al. (2006) is the most complete analysis of velocity gradients in Galactic molecular clouds. Using ^{13}CO $J = 1$–0 emission from the BU-FCRAO GRS, they identified over 500 clouds as topological surfaces above a main beam temperature threshold of 2 K. With the set of voxels for a given cloud, they derived cloud elongations, major axis position angles, velocity gradients, and position angles of the implied rotational axis. The typical velocity gradient, dv/dr, is 0.15 km s^{-1} pc^{-1}, and the orientations of cloud rotational axes follow a uniform distribution. In contrast, most of the identified clouds are elongated with major axes preferentially aligned along the plane of the Galaxy. The random orientation between the rotational and major axes of clouds implies a limited role of angular momentum in shaping the large-scale gas distribution of the cloud.

Imara & Blitz (2011) examined the large-scale velocity fields of several molecular clouds in the Solar Neighborhood using ^{13}CO emission and the atomic halo of each cloud as traced by 21-cm line emission. The inferred angular momentum of the atomic gas is 3–6 times larger than that of the embedded molecular cloud. In most cases, the rotational axes of the atomic gas and molecular clouds are misaligned. These results suggest that a braking mechanism operates between these regimes that redistributes most of the large-scale angular momentum to inertial components not linked to the molecular cloud or that the observed ordered motions in the atomic gas arise from converging flows rather than rotation.

6. CLOUD EVOLUTION AND LIFETIMES

"You don't know what you're talking about!"

"No, *you* don't know what *you're* talking about!"

—Phil Solomon and Pat Thaddeus debating cloud lifetimes at a meeting, circa 1980

The mean time over which a molecular cloud remains a coherent entity capable of generating newborn stars is a key factor in descriptions of star formation and galaxy evolution. This mean cloud lifetime, $\tau_{\rm MC}$, has been a contested issue for over 30 years (Blitz & Shu 1980) and remains unsettled to this day (Ballesteros-Paredes & Hartmann 2007, Scoville 2013). However, $\tau_{\rm MC}$ holds the key to

addressing many important questions related to the ISM and star formation. Do molecular clouds require support against their own self-gravity for many free-fall times? Is there a typical delay before star formation commences within a cloud? What processes are responsible for ultimately destroying a molecular cloud?

In this section, we summarize the arguments for mean molecular cloud lifetimes on the basis of observational data rather than on timescales derived from theory or computational simulations of cloud evolution. However, there are basic principles to which any interpretation of the data must adhere. The formation and destruction of molecular hydrogen can be highly asymmetric in time. Long timescales are required to build up H_2 gas fractions in the low-density regime of the atomic, diffuse gas, but H_2 can be rapidly destroyed by exposure to FUV radiation. Goldsmith & Li (2005) examined the H_2 formation timescale but only considered cosmic-ray ionization of molecular hydrogen that occurs in the strongly self-shielded regime of molecular clouds. The resultant time constant to convert H atoms to H_2 is $2.6/n_{0,3}$ Myr, in which $n_{0,3}$ is the mean hydrogen cloud density, $n_{\rm HI} + 2n_{\rm H2}$, in units of 10^3 cm^{-3}. The time required for the molecular hydrogen within the cloud to reach its steady-state density is $>10^7$ years. This timescale is not the cloud lifetime but is simply the time required to build up significant H_2 mass fractions. The timescale of H_2 formation can be shorter in regions with high gas density that may arise in shells of swept-up atomic gas driven by HII regions, stellar winds, or supernovae or within zones of compressed gas created by shocks of convergent, supersonic gas streams (Glover & Mac Low 2007, Clark et al. 2012, Smith et al. 2014). Proposals that rapidly destroy molecular clouds must also consider the extended timescale required to replace these clouds or else create an imbalance of HI to H_2 mass in the Galaxy.

Estimates of cloud lifetimes are based on the large-scale distribution of H_2 with respect to the atomic and ionized gas components, the arm to interarm contrast in spiral galaxies, and the duty cycle of star formation within clouds. A lower limit to a cloud lifetime is given by its free-fall time, $\tau_{ff} = (3\pi/32{\rm G}\rho)^{1/2} = 0.98 n_{0,3}^{-1/2}$ Myr. The free-fall time is 2 Myr for a mean cloud density of 250 cm^{-3}.

One argument for long molecular lifetimes is based simply on conservation of interstellar mass (Scoville & Hersh 1979). If hydrogen protons continuously cycle through atomic, molecular, and ionized phases, and small losses due to star formation and small gains due to gas infall from the halo are neglected, then

$$\frac{M_{\rm mol}}{\tau_{\rm mol}} \approx \frac{M_{\rm HI+HII}}{\tau_{\rm HI+HII}}, \tag{4}$$

where $M_{\rm mol}$ and $M_{\rm HI+HII}$ are the masses of molecules and atoms+ions, respectively, and $\tau_{\rm mol}$ and $\tau_{\rm HI+HII}$ are the timescales in which hydrogen is in the molecular and atomic+ion phases, respectively. As discussed in Section 4.1, early estimates of the inner Galaxy H_2 mass varied considerably. The higher values of $\sim 4 \times 10^9$ M$_\odot$ (Solomon et al. 1979) suggested a dominance of H_2 over HI in that region. On the basis of such high values and assuming that $\tau_{\rm HI+HII}$ is comparable with an orbital period, $\sim 10^8$ years, in the inner Galaxy, Scoville & Hersh (1979) argued that the time for hydrogen to remain in the molecular gas phase must be significantly longer than 10^8 years. More recent estimates of the inner Galaxy H_2 mass are much lower ($\sim 0.7 \times 10^9$ M$_\odot$; see Section 4.6), and a recent analysis of the Leiden/Argentine/Bonn HI survey suggests that the inner Galaxy HI mass may be significantly higher than has normally been assumed, $\sim 1.8 \times 10^9$ M$_\odot$ (Kalberla & Dedes 2008). Even adopting the lower HI mass of 0.7×10^9 M$_\odot$ derived by Nakanishi & Sofue (2006), the inner Galaxy H_2 mass is at most only comparable with the HI mass and may even be smaller by a factor of a few. Therefore, based on current estimates, mass conservation argues for an H_2 lifetime of 10^8 years or less.

Another argument that has been used to support both long (Scoville & Hersh 1979) and intermediate (Cohen et al. 1980) cloud lifetimes is based on the confinement of molecular clouds to the spiral arms. If broadly distributed with respect to the arms, molecular clouds or fragments must remain intact over the time required to reach the subsequent arm. If these molecular entities survive several spiral arm crossings, then the H_2 lifetime could be longer than an orbital period of $\sim 10^8$ years. We argue in Section 4.4 that molecular clouds are largely confined to the spiral arms, which would imply a cloud lifetime of a few $\times 10^7$ years, the arm crossing time in the inner Galaxy. However this remains a controversial subject, mainly because it is at present impossible to determine accurate distances to the population of generally small and cold clouds that some have argued lie between the arms (Solomon & Rivolo 1989). Although individual molecular clouds have clearly been identified in the interarm regions of the nearby spiral M51 (Koda et al. 2009, Schinnerer et al. 2013), the ISM of that galaxy is so dominated by H_2 (Walter et al. 2008, Koda et al. 2009) that mass conservation would predict that molecular clouds linger in the interarm regions there, even if they do not in the Milky Way.

Arguments for very short cloud lifetimes, $\tau_{MC} \sim \tau_{ff}$, are based on the ages of clusters and newborn stars that are associated with molecular gas. Elmegreen (2000) found that the age and size of clusters in the Large Magellanic Cloud are aligned with the relationship between the cloud crossing time and size. The similarity of cluster ages and cloud crossing time for a fixed spatial scale suggests that star formation is rapid, and molecular cloud lifetimes are correspondingly short. Hartmann et al. (2001) and Ballesteros-Paredes & Hartmann (2007) present additional evidence for rapid cloud evolution and star formation. Most molecular clouds in the Solar Neighborhood are associated with newborn stars with ages less than 3 Myr, whereas young stellar clusters with ages greater than 5 Myr are not coincident with CO emission. Moreover, these clouds are missing a population of 3–10 Myr post-pre-main-sequence stars so the current star-formation activity is the first and perhaps only epoch of stellar production in these regions. This evidence favors an evolutionary sequence in which star formation is initiated or triggered soon after or as part of the formation of the molecular cloud. Once massive stars form, stellar winds and FUV radiation rapidly disperse or displace any remaining molecular gas and, hence, terminate any subsequent production of newborn stars. These arguments are limited to the set of star-forming regions within 1 kpc of the Sun, where there is sufficient X-ray sensitivity to exclude a population of post-pre-main-sequence stars.

Intermediate cloud lifetimes of 10–30 Myr are inferred by the degree of molecular gas linked with Galactic young, open clusters with well-defined stellar ages. Early studies by Bash et al. (1977) and Leisawitz et al. (1989) found molecular structures with mass greater than $10^4\,M_\odot$ associated with all open clusters younger than 5 Myr. In contrast, those clusters with ages greater than 10 Myr retained little or no molecular material as the parent cloud was dispersed or displaced by the effects of the massive star population. A similar track of cloud evolution is compiled by Fukui et al. (1999) and Kawamura et al. (2009) based on CO studies of molecular clouds in the Large Magellanic Cloud. They identify three classes of molecular clouds that they attribute to an evolutionary sequence: Class 1 clouds possess no signatures of massive star formation and represent the earliest stage; Class 2 clouds are linked to a limited number of embedded, compact radio HII regions but with Hα luminosities less than 10^{37} ergs sec^{-1}; and Class 3 clouds harbor young stellar clusters with Hα luminosities greater than 10^{37} ergs sec^{-1}. From their estimate of the timescale to disrupt Class 3 clouds (7 Myr) and the respective fractions of Class 1 and Class 2 clouds that reflect the time duration in each stage (6 and 13 Myr, respectively), they derive a total cloud lifetime of $\sim$25 Myr. This evolutionary sequence is supported by the slow assembly time for stellar clusters within molecular clouds that is inferred from the age spread of cluster members and the absence of significant substructure (Tan et al. 2006).

Murray (2011) examined 32 GMC complexes associated with the 40 most luminous star-forming regions identified by the Wilkinson Microwave Anisotropy Probe that account for 30% of the current star formation in the Milky Way. The duty cycle of photoionizing clusters with respect to a cloud lifetime scales as the number of identified clouds (32) to the number of clouds drawn from the molecular cloud population with sufficient mass to account for the measured fraction of star formation. Assuming molecular clouds are disrupted by feedback from massive stars and a mean cluster age, $<\tau_{ms}>$, of 3.9 Myr, Murray (2011) estimates τ_{MC} of 27 ± 12 Myr. These intermediate cloud lifetimes are supported by theoretical studies that estimate the photoevaporation timescale of 10–30 Myr for GMCs with masses greater than 10^5 $M_\odot$ (Williams & McKee 1997, Matzner 2002).

Estimates of cloud lifetimes based on the duty cycle of star formation exclude the time interval between the formation of the cloud and the initiation of star formation. During this early, dormant phase of cloud evolution, it may have insufficient self-shielding to sustain CO abundances to levels that can be detected in surveys. Mouschovias et al. (2006) considered the spatial displacement between the spiral shock region, traced by dust lanes in which molecular clouds develop, and CO emission coincident with signatures of massive star formation located downstream from the spiral shock. In M51 and M81, the time interval to traverse this distance is 10 Myr and corresponds to a time delay between the initial formation of the cloud and the onset of massive star production. A natural explanation for this delay of star formation in molecular clouds is the time needed for ambipolar diffusion to increase the mass to magnetic flux ratio from an initial subcritical state (Mouschovias 1987).

7. SUMMARY

Over the past twenty years, observational campaigns have provided an extensive inventory of molecular gas in the Milky Way through measurements of CO $J = 1$–0 emission, near-IR imagery, and thermal dust radiation with angular resolutions between 0.25 arcmin and 8 arcmin. These accomplishments have been complemented by both numerical simulations of the complex evolution of molecular clouds and fundamental analytical theory that keeps the interpretation of data and simulations grounded in physics. The current CO surveys continue to be used extensively to interpret data collected at other wavelengths—both as a measure of H_2 column density in self-shielded environments and as velocity tags to sources identified in photometric surveys. More importantly, these data have resolved long-standing debates on the large-scale distribution of H_2 in the Galaxy and molecular cloud lifetimes. Detailed imaging of CO emission in nearby clouds reveals the complex interplay between gravity, magnetic fields, and turbulence.

SUMMARY POINTS

1. The mass of H_2 gas in the Milky Way is $1.0 \pm 0.3 \times 10^9$ $M_\odot$. This value is derived from CO surveys assuming $X_{CO} = 2 \times 10^{20}$ molecules cm^{-2} (K km s^{-1})$^{-1}$, $R_{Sun} = 8.5$ kpc, and does not include the mass of associated helium. Most of the H_2 gas (60–70%) is located inside the solar circle.
2. The H_2 gas is largely confined to the plane of the Galaxy within a Gaussian layer with full width at half maximum thickness of 90 pc in the inner Galaxy that subsequently broadens to several hundred parsecs for radii greater than 10 kpc.
3. Molecular gas is mainly confined to the Galactic spiral arms.

4. The concentration of molecular clouds in spiral arms and an H_2-to-HI mass ratio of at most unity in the inner Galaxy and much less in the outer Galaxy implies an upper limit to cloud lifetimes of 10^8 years. The duty cycle of star formation within molecular clouds imply lifetimes <30 Myr.
5. Both ^{12}CO emission, with a constant value of X_{CO}, and optically thin ^{13}CO emission show that the mass surface density of molecular clouds decreases with increasing Galactic radius.
6. Scaling relationships between velocity dispersion, size, and surface density indicate that molecular clouds are gravitationally bound.
7. Observations of hierarchical structure, log-normal probability density functions of gas column density, and the functional form of velocity structure functions all point to the ubiquity of compressible magnetohydrodynamic turbulent flows within molecular clouds.
8. Velocity structure functions of clouds with comparable mass surface densities are aligned. This universality connects the turbulent motions within clouds to the line width–size relationship among clouds and points to a cloud formation process from the atomic gas substrate of the ISM that is common to all clouds.

FUTURE ISSUES

Although much progress has been made from the analysis of CO data, two pivotal issues require attention from astronomers in the coming years: more precise measures of cloud lifetimes and the role of stellar feedback on molecular clouds. In this review, we advocate an upper limit to the cloud lifetimes of 10^8 years. Yet, this limit does not significantly constrain rather divergent descriptions of cloud evolution related to very short and intermediate cloud lifetimes. Short cloud lifetimes imply that star formation is rapid, all clouds are in a state of gravitational collapse, and feedback from the stellar winds and HII regions of newborn massive stars efficiently quenches any subsequent production of stars. But, are clouds globally or hierarchically collapsing? What are the kinematic signatures of such collapse that can be distinguished from the effects of turbulent motions? Computational simulations and synthetic observations of the model velocity and density fields can contribute to the development of such observational signatures. Intermediate cloud lifetimes require support of the cloud against its own self gravity and sufficient inertia to prevent its rapid dispersal by stellar winds and expanding HII regions. Therefore, the role of momentum and energy feedback from newborn stars is coupled to the issue of cloud lifetimes. Feedback from young stars can influence subsequent star formation within the cloud (both positively and negatively) and modulate the density and velocity structure of the cloud; it may ultimately be responsible for the dispersal of the cloud itself. How can the observations quantify the effects of such feedback processes on cloud evolution?

The Atacama Large Millimeter Array (ALMA) is expected to play a major role in observational investigations of the molecular ISM in the Milky Way. The angular resolution of ALMA at 115 GHz ranges from 3.5 arcsec with its most compact configuration, 0.5 arcsec with 1-km baselines, and 0.03 arcsec in its most extended 16-km baseline. In the Milky Way, ALMA can resolve small-scale, high-density structures within clouds at large distances in

the disk of the Galaxy and the Galactic Center. This capability enables direct comparisons with the well-studied local clouds on which much of our understanding of the star-formation process is based. However, with reduced sensitivity to extended, low surface brightness emission with increasing baselines, ALMA does not effectively probe the low column density substrate of molecular clouds. Inclusion of the Atacama Compact Array and total power auxiliary measurements with the full array can recover this component to scales ~50 times greater than these resolutions but at the expense of longer integration times. At a distance of 10 Mpc, ALMA can resolve spatial scales ranging from 170 to 1.5 pc. Thus, ALMA can extend many of the analyses discussed in this review to molecular clouds residing within nearby galaxies (Bolatto et al. 2008, Colombo et al. 2014, Leroy et al. 2015).

The extended, low surface brightness domain of molecular clouds in the Milky Way shall remain best studied by single-dish, filled-aperture systems, preferably equipped with heterodyne focal plane arrays. Current moderate- to large-size single-dish telescopes capable of wide-field imaging of the low-*J* transitions of CO in order of increasing aperture diameter are the Atacama Submillimeter Telescope Experiment 10-m, the Arizona Radio Observatory 10-m and 12-m, the Atacama Pathfinder Experiment 12-m, the Delingha 13.7-m, the Mopra 22-m, the Institut de Radio Astronomie Millimétrique 30-m, the Large Millimeter Telescope 32-m (to be upgraded to 50 m), the refurbished Haystack 37-m, the Nobeyama 45-m, and the Green Bank Telescope 100-m telescopes.

Finally, the molecular ISM can be further explored with novel analysis methods that exploit the rich information that resides within current and future data. Collaborations of astronomers with computer and statistical scientists to explore large, complicated data sets can lead to new analyses and insights in which conventional assumptions or convenient definitions are relaxed.

DISCLOSURE STATEMENT

The authors are not aware of any affiliations, memberships, funding, or financial holdings that might be perceived as affecting the objectivity of this review.

ACKNOWLEDGMENTS

The authors are grateful for comments from Chris McKee, Neal Evans, Paul Goldsmith, Edith Falgarone, Stella Offner, Jay Lockman, Loris Magnani, Leo Blitz, Chris Brunt, Alyssa Goodman, Leonardo Bronfman, Ewine van Dishoeck, Joseph Mottram, and Andreas Schruba. Y. Fukui kindly provided the NANTEN data included in **Figure 3**. M.H. acknowledges support from the Max Planck Institute for Radio Astronomy in Bonn and the Collaborative Research Center 956, funded by the Deutsche Forschungsgemeinschaft and from grant NSF-AST1009049. T.M.D. acknowledges the many graduate students and postdocs whose work contributed to the Columbia–University of Chile–Center for Astrophysics Galactic CO survey and salutes his career-long mentor Patrick Thaddeus, whose foresight led to many of the results summarized in this work.

LITERATURE CITED

Acharyya K, Fuchs GW, Fraser HJ, van Dishoeck EF, Linnartz H. 2007. *Astron. Astrophys.* 466:1005–12
Ackermann M, Ajello M, Atwood WB, et al. 2012. *Ap. J.* 750:3
Aguirre JE, Ginsburg AG, Dunham MK, et al. 2011. *Ap. J. Suppl.* 192:4

Allen RJ, Rodríguez MI, Black JH, Booth RS. 2012. *Astron. J.* 143:97
Alves J, Lombardi M, Lada CJ. 2007. *Astron. Astrophys.* 462:L17–21
Anderson LD, Bania TM, Balser DS, Rood RT. 2012. *Ap. J.* 754:62
André P, Men'shchikov A, Bontemps S, et al. 2010. *Astron. Astrophys.* 518:L102
Arnaud K, Riley PA, Wolfendale AW, et al. 1982. *MNRAS* 201:745–58
Arzoumanian D, André P, Peretto N, Könyves V. 2013. *Astron. Astrophys.* 553:A119
Ballesteros-Paredes J, Hartmann L. 2007. *Rev. Mex. Astron. Astrofis.* 43:123–36
Ballesteros-Paredes J, Hartmann LW, Vázquez-Semadeni E, Heitsch F, Zamora-Avilés MA. 2011. *MNRAS* 411:65–70
Bally J, Langer WD, Stark AA, Wilson RW. 1987. *Ap. J. Lett.* 312:L45–49
Balser DS, Rood RT, Bania TM, Anderson LD. 2011. *Ap. J.* 738:27
Bania TM. 1977. *Ap. J.* 216:381–403
Bania TM. 1980. *Ap. J.* 242:95–111
Barnard EE, Frost EB, Calvert MR. 1927. *A Photographic Atlas of Selected Regions of the Milky Way*. Washington, DC: Carnegie Inst. Wash.
Barnes PJ, Muller E, Indermühle B, et al. 2015. *Ap. J.* In press
Bash FN, Green E, Peters WL III. 1977. *Ap. J.* 217:464–72
Battisti AJ, Heyer MH. 2014. *Ap. J.* 780:173
Beaumont CN, Offner SSR, Shetty R, Glover SCO, Goodman AA. 2013. *Ap. J.* 777:173
Bergin EA, Langer WD, Goldsmith PF. 1995. *Ap. J.* 441:222–43
Bergin EA, Tafalla M. 2007. *Annu. Rev. Astron. Astrophys.* 45:339–96
Bertoldi F, McKee CF. 1992. *Ap. J.* 395:140–57
Bitran M, Alvarez H, Bronfman L, May J, Thaddeus P. 1997. *Astron. Astrophys. Suppl.* 125:99–138
Blair GN, Evans NJ II, Vanden Bout PA, Peters WL III. 1978. *Ap. J.* 219:896
Blitz L, Bazell D, Desert FX. 1990. *Ap. J. Lett.* 352:L13–16
Blitz L, Bloemen JBGM, Hermsen W, Bania TM. 1985. *Astron. Astrophys.* 143:267–73
Blitz L, Fich M, Stark AA. 1982. *Ap. J. Suppl.* 49:183–206
Blitz L, Magnani L, Mundy L. 1984. *Ap. J. Lett.* 282:L9–12
Blitz L, Shu FH. 1980. *Ap. J.* 238:148–57
Blitz L, Thaddeus P. 1980. *Ap. J.* 241:676–96
Bloemen JBGM, Strong AW, Mayer-Hasselwander HA, et al. 1986. *Astron. Astrophys.* 154:25–41
Boggess NW, Mather JC, Weiss R, et al. 1992. *Ap. J.* 397:420–29
Bolatto AD, Leroy AK, Rosolowsky E, Walter F, Blitz L. 2008. *Ap. J.* 686:948–65
Bolatto AD, Wolfire M, Leroy AK. 2013. *Annu. Rev. Astron. Astrophys.* 51:207–68
Boldyrev S. 2002. *Ap. J.* 569:841–45
Boulanger F, Baud B, van Albada GD. 1985. *Astron. Astrophys.* 144:L9–12
Brand J, Wouterloot JGA. 1994. *Astron. Astrophys. Suppl.* 103:503–40
Brand J, Wouterloot JGA. 1995. *Astron. Astrophys.* 303:851
Bronfman L, Cohen RS, Alvarez H, May J, Thaddeus P. 1988. *Ap. J.* 324:248–66
Brunt CM. 2003. *Ap. J.* 584:293–315
Brunt CM. 2010. *Astron. Astrophys.* 513:A67
Brunt CM, Federrath C, Price DJ. 2010a. *MNRAS* 405:L56–60
Brunt CM, Federrath C, Price DJ. 2010b. *MNRAS* 403:1507–15
Brunt CM, Heyer MH. 2002a. *Ap. J.* 566:276–88
Brunt CM, Heyer MH. 2002b. *Ap. J.* 566:289–301
Brunt CM, Heyer MH. 2013. *MNRAS* 433:117–26
Brunt CM, Heyer MH, Mottram JC, Douglas KA, Summers LJ. 2015. *MNRAS.* In press
Brunt CM, Kerton CR, Pomerleau C. 2003. *Ap. J. Suppl.* 144:47–70
Buckle JV, Curtis EI, Roberts JF, et al. 2010. *MNRAS* 401:204–22
Burton MG, Braiding C, Glueck C, et al. 2013. *Publ. Astron. Soc. Aust.* 30:44
Burton WB. 1971. *Astron. Astrophys.* 10:76
Burton WB, Gordon MA. 1978. *Astron. Astrophys.* 63:7–27
Burton WB, Gordon MA, Bania TM, Lockman FJ. 1975. *Ap. J.* 202:30–49

Carlhoff P, Nguyen Luong Q, Schilke P, et al. 2013. *Astron. Astrophys.* 560:A24
Carpenter JM, Snell RL, Schloerb FP. 1995. *Ap. J.* 445:246–68
Carr JS. 1987. *Ap. J.* 323:170–78
Carruthers GR. 1970. *Ap. J. Lett.* 161:L81
Casoli F, Combes F, Gerin M. 1984. *Astron. Astrophys.* 133:99–109
Chabrier G. 2003. *Publ. Astron. Soc. Pac.* 115:763–95
Cheung AC, Rank DM, Townes CH, Thornton DD, Welch WJ. 1968. *Phys. Rev. Lett.* 21:1701–5
Cheung AC, Rank DM, Townes CH, Thornton DD, Welch WJ. 1969. *Nature* 221:626–28
Chi S, Park YS. 2006. *J. Korean Astron. Soc.* 39:19–24
Clark PC, Glover SCO, Klessen RS, Bonnell IA. 2012. *MNRAS* 424:2599–613
Clemens DP, Sanders DB, Scoville NZ. 1988. *Ap. J.* 327:139–55
Cohen RS, Cong H, Dame TM, Thaddeus P. 1980. *Ap. J. Lett.* 239:L53–56
Cohen RS, Dame TM, Thaddeus P. 1986. *Ap. J. Suppl.* 60:695–818
Cohen RS, Thaddeus P. 1977. *Ap. J. Lett.* 217:L155–59
Colombo D, Hughes A, Schinnerer E, et al. 2014. *Ap. J.* 784:3
Combes F. 1991. *Annu. Rev. Astron. Astrophys.* 29:195–237
Crutcher RM. 1999. *Ap. J.* 520:706–13
Crutcher RM. 2012. *Annu. Rev. Astron. Astrophys.* 50:29–63
Crutcher RM, Wandelt B, Heiles C, Falgarone E, Troland TH. 2010. *Ap. J.* 725:466–79
Dame TM. 1983. *Molecular clouds and galactic spiral structure*. PhD Thesis, Columbia Univ., New York
Dame TM. 1993. In *Back to the Galaxy*, ed. SS Holt, F Verter. *AIP Conf. Ser.* 278:267–78. Melville, NY: AIP
Dame TM, Elmegreen BG, Cohen RS, Thaddeus P. 1986. *Ap. J.* 305:892–908
Dame TM, Hartmann D, Thaddeus P. 2001. *Ap. J.* 547:792–813
Dame TM, Thaddeus P. 1985. *Ap. J.* 297:751–65
Dame TM, Thaddeus P. 1994. *Ap. J. Lett.* 436:L173–76
Dame TM, Thaddeus P. 2004. In *Milky Way Surveys: The Structure and Evolution of Our Galaxy*, ed. D Clemens, R Shah, T Brainerd. *ASP Conf. Ser.* 317:66. San Francisco: ASP
Dame TM, Ungerechts H, Cohen RS, et al. 1987. *Ap. J.* 322:706–20
Dent WRF, Hovey GJ, Dewdney PE, et al. 2009. *MNRAS* 395:1805–21
Desert FX, Bazell D, Boulanger F. 1988. *Ap. J.* 334:815–40
Dickey JM, Crovisier J, Kazes I. 1981. *Astron. Astrophys.* 98:271–85
Dickey JM, McClure-Griffiths NM, Gaensler BM, Green AJ. 2003. *Ap. J.* 585:801–22
Dickman RL. 1975. *Ap. J.* 202:50–57
Dickman RL. 1978. *Ap. J. Suppl.* 37:407–27
Digel S, Thaddeus P, Bally J. 1990. *Ap. J. Lett.* 357:L29–33
Digel SW. 1991. *Molecular clouds in the distant outer galaxy*. PhD Thesis, Harvard Univ., Cambridge, MA
Digel SW, Lyder DA, Philbrick AJ, Puche D, Thaddeus P. 1996. *Ap. J.* 458:561
Dobashi K, Bernard JP, Fukui Y. 1996. *Ap. J.* 466:282
Dobashi K, Bernard JP, Yonekura Y, Fukui Y. 1994. *Ap. J. Suppl.* 95:419–56
Dobbs CL, Burkert A. 2012. *MNRAS* 421:2940–46
Dobbs CL, Burkert A, Pringle JE. 2011. *MNRAS* 417:1318–34
Elmegreen BG. 2000. *Ap. J.* 530:277–81
Elmegreen BG. 2002. *Ap. J.* 564:773–81
Elmegreen BG, Falgarone E. 1996. *Ap. J.* 471:816
Elmegreen BG, Scalo J. 2004. *Annu. Rev. Astron. Astrophys.* 42:211–73
Englmaier P, Gerhard O. 1999. *MNRAS* 304:512–34
Erickson NR, Grosslein RM, Erickson RB, Weinreb S. 1999. *IEEE Trans. Microw. Theory Tech.* 47:2212–19
Esquivel A, Lazarian A. 2005. *Ap. J.* 631:320–50
Falgarone E, Pety J, Hily-Blant P. 2009. *Astron. Astrophys.* 507:355–68
Falgarone E, Puget JL, Perault M. 1992. *Astron. Astrophys.* 257:715–30
Federman SR, Glassgold AE, Kwan J. 1979. *Ap. J.* 227:466–73
Field GB, Blackman EG, Keto ER. 2011. *MNRAS* 416:710–14
Frerking MA, Langer WD, Wilson RW. 1982. *Ap. J.* 262:590–605

Froebrich D, Rowles J. 2010. *MNRAS* 406:1350–57
Fukui Y, Kawamura A. 2010. *Annu. Rev. Astron. Astrophys.* 48:547–80
Fukui Y, Mizuno N, Yamaguchi R, et al. 1999. *Publ. Astron. Soc. Jpn.* 51:745–49
Fukui Y, Okamoto R, Kaji R, et al. 2014. *Ap. J.* 796:59
Fux R. 1999. *Astron. Astrophys.* 345:787–812
García P, Bronfman L, Nyman LÅ, Dame TM, Luna A. 2014. *Ap. J. Suppl.* 212:2
Garcia-Burillo S, Guelin M, Cernicharo J, Dahlem M. 1992. *Astron. Astrophys.* 266:21–36
Glover SCO, Mac Low MM. 2007. *Ap. J.* 659:1317–37
Goldreich P, Kwan J. 1974. *Ap. J.* 189:441–54
Goldsmith PF. 1987. In *Interstellar Processes*, ed. DJ Hollenbach, HA Thronson Jr., 134:51–70. *Ap. Space Sci. Libr.* Dordrecht, Neth.: Reidel
Goldsmith PF, Heyer M, Narayanan G, et al. 2008. *Ap. J.* 680:428–45
Goldsmith PF, Li D. 2005. *Ap. J.* 622:938–58
Goodman AA, Barranco JA, Wilner DJ, Heyer MH. 1998. *Ap. J.* 504:223
Goodman AA, Pineda JE, Schnee SL. 2009. *Ap. J.* 692:91–103
Gordon MA, Burton WB. 1976. *Ap. J.* 208:346–53
Gould RJ, Salpeter EE. 1963. *Ap. J.* 138:393
Grabelsky DA, Cohen RS, Bronfman L, Thaddeus P. 1988. *Ap. J.* 331:181–96
Grabelsky DA, Cohen RS, Bronfman L, Thaddeus P, May J. 1987. *Ap. J.* 315:122–41
Grenier IA, Casandjian JM, Terrier R. 2005. *Science* 307:1292–95
Hachisuka K, Brunthaler A, Menten KM, et al. 2009. *Ap. J.* 696:1981–86
Hartmann D, Burton WB. 1997. *Atlas of Galactic Neutral Hydrogen.* Cambridge, UK: Cambridge Univ. Press
Hartmann D, Magnani L, Thaddeus P. 1998. *Ap. J.* 492:205–12
Hartmann L, Ballesteros-Paredes J, Bergin EA. 2001. *Ap. J.* 562:852–68
Heiles C. 1969. *Ap. J.* 156:493
Hennebelle P, Chabrier G. 2008. *Ap. J.* 684:395–410
Hennebelle P, Falgarone E. 2012. *Astron. Astrophys. Rev.* 20:55
Heyer M, Krawczyk C, Duval J, Jackson JM. 2009. *Ap. J.* 699:1092–103
Heyer MH, Brunt C, Snell RL, et al. 1998. *Ap. J. Suppl.* 115:241
Heyer MH, Brunt CM. 2004. *Ap. J. Lett.* 615:L45–48
Heyer MH, Carpenter JM, Snell RL. 2001. *Ap. J.* 551:852–66
Heyer MH, Schloerb FP. 1997. *Ap. J.* 475:173
Heyer MH, Terebey S. 1998. *Ap. J.* 502:265–77
Heyer MH, Williams JP, Brunt CM. 2006. *Ap. J.* 643:956–64
Hily-Blant P, Falgarone E, Pety J. 2008. *Astron. Astrophys.* 481:367–80
Hollenbach D, Salpeter EE. 1971. *Ap. J.* 163:155
Hollenbach DJ, Werner MW, Salpeter EE. 1971. *Ap. J.* 163:165
Honma M, Nagayama T, Ando K, et al. 2012. *Publ. Astron. Soc. Jpn.* 64:136
Hunter SD, Bertsch DL, Catelli JR, et al. 1997. *Ap. J.* 481:205–40
Imara N, Blitz L. 2011. *Ap. J.* 732:78
Israel FP, de Graauw T, van der Biezen J, et al. 1984. *Astron. Astrophys.* 134:396–401
Issa M, MacLaren I, Wolfendale AW. 1990. *Ap. J.* 352:132–38
Jackson JM, Rathborne JM, Shah RY, et al. 2006. *Ap. J. Suppl.* 163:145–59
Jacq T, Baudry A, Walmsley CM. 1988. *Astron. Astrophys.* 207:145–53
Kainulainen J, Beuther H, Henning T, Plume R. 2009. *Astron. Astrophys.* 508:L35–38
Kainulainen J, Ragan SE, Henning T, Stutz A. 2013. *Astron. Astrophys.* 557:A120
Kainulainen J, Tan JC. 2013. *Astron. Astrophys.* 549:A53
Kalberla PMW, Dedes L. 2008. *Astron. Astrophys.* 487:951–63
Kalberla PMW, Kerp J. 2009. *Annu. Rev. Astron. Astrophys.* 47:27–61
Kato S, Mizuno N, Asayama S-i, et al. 1999. *Publ. Astron. Soc. Jpn.* 51:883–93
Kawamura A, Mizuno Y, Minamidani T, et al. 2009. *Ap. J. Suppl.* 184:1–17
Kawamura A, Onishi T, Yonekura Y, et al. 1998. *Ap. J. Suppl.* 117:387
Kazès I, Crovisier J. 1981. *Astron. Astrophys.* 101:401–8

Kennicutt RC, Evans NJ. 2012. *Annu. Rev. Astron. Astrophys.* 50:531–608
Keto ER, Myers PC. 1986. *Ap. J.* 304:466–80
Kleiner SC, Dickman RL. 1985. *Ap. J.* 295:466–84
Knapp GR, Stark AA, Wilson RW. 1985. *Astron. J.* 90:254–300
Koda J, Sawada T, Hasegawa T, Scoville NZ. 2006. *Ap. J.* 638:191–95
Koda J, Scoville N, Sawada T, et al. 2009. *Ap. J. Lett.* 700:L132–36
Kolmogorov A. 1941. *Akad. Nauk. SSSR Doklady* 30:301–5
Könyves V, André P, Men'shchikov A, et al. 2010. *Astron. Astrophys.* 518:L106
Kramer C, Stutzki J, Rohrig R, Corneliussen U. 1998. *Astron. Astrophys.* 329:249–64
Krumholz MR. 2014. arXiv:1402.0867
Krumholz MR, McKee CF. 2005. *Ap. J.* 630:250–68
Kulesa CA. 2002. *Molecular hydrogen and its ions in dark interstellar clouds and star forming regions*. PhD Thesis, Univ. Arizona, Tucson
Kutner ML, Mead KN. 1981. *Ap. J. Lett.* 249:L15–18
Kutner ML, Tucker KD, Chin G, Thaddeus P. 1977. *Ap. J.* 215:521–28
Lacy JH, Knacke R, Geballe TR, Tokunaga AT. 1994. *Ap. J. Lett.* 428:L69–72
Lada CJ, Forbrich J, Lombardi M, Alves JF. 2012. *Ap. J.* 745:190
Lada CJ, Lada EA, Clemens DP, Bally J. 1994. *Ap. J.* 429:694–709
Lada CJ, Lombardi M, Alves JF. 2010. *Ap. J.* 724:687–93
Langer WD, Velusamy T, Pineda JL, Willacy K, Goldsmith PF. 2014. *Astron. Astrophys.* 561:A122
Larson RB. 1981. *MNRAS* 194:809–26
Lazarian A, Pogosyan D. 2000. *Ap. J.* 537:720–48
Le Petit F, Nehmé C, Le Bourlot J, Roueff E. 2006. *Ap. J. Suppl.* 164:506–29
Lee Y, Jung JH, Chung HS, et al. 1999. *Astron. Astrophys. Suppl.* 138:187–202
Lee Y, Stark AA, Kim HG, Moon DS. 2001. *Ap. J. Suppl.* 136:137–87
Leisawitz D, Bash FN, Thaddeus P. 1989. *Ap. J. Suppl.* 70:731–812
Leroy AK, Bolatto AD, Ostriker EC, et al. 2015. *Astron. J.* 801:25–52
Leung HO, Thaddeus P. 1992. *Ap. J. Suppl.* 81:267–301
Liszt HS, Burton WB. 1981. *Ap. J.* 243:778–813
Liszt HS, Burton WB, Xiang DL. 1984. *Astron. Astrophys.* 140:303–13
Lombardi M, Alves J, Lada CJ. 2011. *Astron. Astrophys.* 535:A16
Low FJ, Young E, Beintema DA, et al. 1984. *Ap. J. Lett.* 278:L19–22
Lynds BT. 1962. *Ap. J. Suppl.* 7:1
Magnani L. 1994. In *The First Symposium on the Infrared Cirrus and Diffuse Interstellar Clouds*, ed. RM Cutri, WB Latter. *ASP Conf. Ser.* 58:161. San Francisco: ASP
Magnani L, Blitz L, Lada EA. 1986. *Ap. J.* 301:395–97
Magnani L, Blitz L, Mundy L. 1985. *Ap. J.* 295:402–21
Magnani L, Hartmann D, Holcomb SL, Smith LE, Thaddeus P. 2000. *Ap. J.* 535:167–75
Magnani L, Smith AJ. 2010. *Ap. J.* 722:1685–90
Malhotra S. 1994a. *Ap. J.* 437:194–203
Malhotra S. 1994b. *Ap. J.* 433:687–704
Matzner CD. 2002. *Ap. J.* 566:302–14
May J, Bronfman L, Alvarez H, Murphy DC, Thaddeus P. 1993. *Astron. Astrophys. Suppl.* 99:105–65
McClure-Griffiths NM, Dickey JM, Gaensler BM, et al. 2005. *Ap. J. Suppl.* 158:178–87
McCutcheon WH, Robinson BJ, Whiteoak JB. 1981. *Proc. Astron. Soc. Aust.* 4:243–47
McKee CF, Krumholz MR. 2010. *Ap. J.* 709:308–20
McKee CF, Li PS, Klein RI. 2010. *Ap. J.* 720:1612–34
McKee CF, Ostriker EC. 2007. *Annu. Rev. Astron. Astrophys.* 45:565–687
Miesch MS, Bally J. 1994. *Ap. J.* 429:645–71
Miller GE, Scalo JM. 1979. *Ap. J. Suppl.* 41:513–47
Mizuno A, Fukui Y. 2004. In *Milky Way Surveys: The Structure and Evolution of Our Galaxy*, ed. D Clemens, R Shah, T Brainerd. *ASP Conf. Ser.* 317:59. San Francisco: ASP
Moriguchi Y, Yamaguchi N, Onishi T, Mizuno A, Fukui Y. 2001. *Publ. Astron. Soc. Jpn.* 53:1025–36

Motte F, Andre P, Neri R. 1998. *Astron. Astrophys.* 336:150–72
Motte F, Schilke P, Lis DC. 2003. *Ap. J.* 582:277–91
Mottram JC, Brunt CM. 2010. In *The Dynamic Interstellar Medium: A Celebration of the Canadian Galactic Plane Survey*, ed. R Kothes, TL Landecker, AG Willis. *ASP Conf. Ser.* 438:98. San Francisco: ASP
Mouschovias TC. 1987. In *NATO ASIC Proc. 210: Physical Processes in Interstellar Clouds*, ed. GE Morfill, M Scholer, p. 453. Dordrecht, Neth.: Reidel
Mouschovias TC, Spitzer L Jr. 1976. *Ap. J.* 210:326
Mouschovias TC, Tassis K, Kunz MW. 2006. *Ap. J.* 646:1043–49
Murray N. 2011. *Ap. J.* 729:133
Myers PC, Dame TM, Thaddeus P, et al. 1986. *Ap. J.* 301:398–422
Nakanishi H, Sofue Y. 2006. *Publ. Astron. Soc. Jpn.* 58:847–60
Narayanan D, Krumholz MR, Ostriker EC, Hernquist L. 2012. *MNRAS* 421:3127–46
Narayanan G, Heyer MH, Brunt C, et al. 2008. *Ap. J. Suppl.* 177:341–61
Nyman LA, Bronfman L, Thaddeus P. 1989. *Astron. Astrophys.* 216:185–92
Oka T, Hasegawa T, Sato F, et al. 2001. *Ap. J.* 562:348–62
Oliver RJ, Masheder MRW, Thaddeus P. 1996. *Astron. Astrophys.* 315:578–90
Onishi T, Yoshikawa N, Yamamoto H, et al. 2001. *Publ. Astron. Soc. Jpn.* 53:1017–23
Ostriker EC, Stone JM, Gammie CF. 2001. *Ap. J.* 546:980–1005
Padoan P, Nordlund Å. 2002. *Ap. J.* 576:870–79
Passot T, Vázquez-Semadeni E. 1998. *Phys. Rep. E* 58:4501–10
Pettitt AR, Dobbs CL, Acreman DM, Price DJ. 2014. *MNRAS* 444:919–41
Pety J, Schinnerer E, Leroy AK, et al. 2013. *Ap. J.* 779:43
Pineda JE, Caselli P, Goodman AA. 2008. *Ap. J.* 679:481–96
Pineda JL, Goldsmith PF, Chapman N, et al. 2010. *Ap. J.* 721:686–708
Planck, Fermi Collab., Ade PAR, Aghanim N, Aniano G, et al. 2014. arXiv:1409.3268
Planck Collab., Ade PAR, Aghanim N, Alves MIR, et al. 2014. *Astron. Astrophys.* 571:A13
Planck Collab. XIX, Ade PAR, Aghanim N, Arnaud M, et al. 2011. *Astron. Astrophys.* 536:A19
Planck Collab. XXIII, Ade PAR, Aghanim N, Alves MIR, et al. 2014. arXiv:1406.5093
Pohl M, Englmaier P, Bissantz N. 2008. *Ap. J.* 677:283–91
Rathborne JM, Johnson AM, Jackson JM, Shah RY, Simon R. 2009. *Ap. J. Suppl.* 182:131–42
Reach WT, Wall WF, Odegard N. 1998. *Ap. J.* 507:507–25
Reid MJ, Menten KM, Brunthaler A, et al. 2014. *Ap. J.* 783:130
Reid MJ, Menten KM, Zheng XW, et al. 2009. *Ap. J.* 700:137–48
Ridge NA, Di Francesco J, Kirk H, et al. 2006. *Astron. J.* 131:2921–33
Ripple F, Heyer MH, Gutermuth R, Snell RL, Brunt CM. 2013. *MNRAS* 431:1296–313
Robinson BJ, Manchester RN, Whiteoak JB, Otrupcek RE, McCutcheon WH. 1988. *Astron. Astrophys.* 193:60–68
Robinson BJ, Manchester RN, Whiteoak JB, et al. 1984. *Ap. J. Lett.* 283:L31–35
Röllig M, Ossenkopf V, Jeyakumar S, Stutzki J, Sternberg A. 2006. *Astron. Astrophys.* 451:917–24
Roman-Duval J, Federrath C, Brunt C, et al. 2011. *Ap. J.* 740:120
Roman-Duval J, Jackson JM, Heyer M, et al. 2009. *Ap. J.* 699:1153–70
Roman-Duval J, Jackson JM, Heyer M, Rathborne J, Simon R. 2010. *Ap. J.* 723:492–507
Román-Zúñiga CG, Lada CJ, Alves JF. 2009. *Ap. J.* 704:183–95
Rosolowsky E. 2005. *Publ. Astron. Soc. Pac.* 117:1403–10
Rosolowsky E, Leroy A. 2006. *Publ. Astron. Soc. Pac.* 118:590–610
Rosolowsky EW, Pineda JE, Kauffmann J, Goodman AA. 2008. *Ap. J.* 679:1338–51
Sakamoto S, Hasegawa T, Handa T, Hayashi M, Oka T. 1997. *Ap. J.* 486:276–90
Sakamoto S, Hasegawa T, Hayashi M, Handa T, Oka T. 1995. *Ap. J. Suppl.* 100:125
Salpeter EE. 1955. *Ap. J.* 121:161
Sanders DB, Clemens DP, Scoville NZ, Solomon PM. 1986. *Ap. J. Suppl.* 60:1–296
Sanders DB, Solomon PM, Scoville NZ. 1984. *Ap. J.* 276:182–203
Sanna A, Reid MJ, Dame TM, et al. 2012. *Ap. J.* 745:82
Sanna A, Reid MJ, Menten KM, et al. 2014. *Ap. J.* 781:108

Sato K. 1997. In *Millimeter and Submillimeter Astronomy at 10 Milli-arcseconds Resolution, Tokyo, Japan, Mar. 16–19*, ed. M Ishiguro, R Kawabe, pp. 56. Minamimaki, Japan: Nobeyama Radio Obs.
Sato M, Wu YW, Immer K, et al. 2014. *Ap. J.* 793:72
Sawada T, Hasegawa T, Handa T, et al. 2001. *Ap. J. Suppl.* 136:189–219
Scalo J, Elmegreen BG. 2004. *Annu. Rev. Astron. Astrophys.* 42:275–316
Scalo JM. 1984. *Ap. J.* 277:556–61
Scalo JM. 1985. In *Protostars and Planets II*, ed. DC Black, MS Matthews, pp. 201–96. Tucson: Univ. Ariz. Press
Schinnerer E, Meidt SE, Pety J, et al. 2013. *Ap. J.* 779:42
Schloerb FP, Snell RL. 1984. *Ap. J.* 283:129–39
Schmidt M. 1956. *Bull. Astron. Inst. Neth.* 13:15
Schneider N, Bontemps S, Simon R, et al. 2006. *Astron. Astrophys.* 458:855–71
Schneider N, Bontemps S, Simon R, et al. 2011. *Astron. Astrophys.* 529:A1
Schneider N, Brooks K. 2004. *Publ. Astron. Soc. Aust.* 21:290–301
Schneider N, Ossenkopf V, Csengeri T, et al. 2015. *Astron. Astrophys.* 575:79–95
Schuller F, Menten KM, Contreras Y, et al. 2009. *Astron. Astrophys.* 504:415–27
Schuster KF, Boucher C, Brunswig W, et al. 2004. *Astron. Astrophys.* 423:1171–77
Schwartz PR, Wilson WJ, Epstein EE. 1973. *Ap. J.* 186:529–36
Scoville NZ. 2013. In *Secular Evolution Galaxies*, ed. J Falcón-Barroso, JH Knapen, pp. 491–554. Cambridge, UK: Cambridge Univ. Press
Scoville NZ, Hersh K. 1979. *Ap. J.* 229:578–82
Scoville NZ, Solomon PM. 1975. *Ap. J. Lett.* 199:L105–9
Scoville NZ, Yun MS, Sanders DB, Clemens DP, Waller WH. 1987. *Ap. J. Suppl.* 63:821–915
Shane WW. 1972. *Astron. Astrophys.* 16:118
Sharpless S. 1959. *Ap. J. Suppl.* 4:257
She ZS, Leveque E. 1994. *Phys. Rev. Lett.* 72:336–39
Sheffer Y, Rogers M, Federman SR, et al. 2008. *Ap. J.* 687:1075–106
Shetty R, Beaumont CN, Burton MG, Kelly BC, Klessen RS. 2012. *MNRAS* 425:720–29
Shimajiri Y, Kawabe R, Takakuwa S, et al. 2011. *Publ. Astron. Soc. Jpn.* 63:105–23
Simon R, Jackson JM, Clemens DP, Bania TM, Heyer MH. 2001. *Ap. J.* 551:747–63
Smith H, Buckle J, Hills R, et al. 2008. In *Millimeter and Submillimeter Detectors and Instrumentation for Astronomy IV*, ed. WD Duncan, WS Holland, S Withington, J Zmuidzinas. *Proc. SPIE Conf. Ser.* 7020:70200Z. Bellingham, WA: SPIE
Smith RJ, Glover SCO, Clark PC, Klessen RS, Springel V. 2014. *MNRAS* 441:1628–45
Snyder LE, Buhl D, Zuckerman B, Palmer P. 1969. *Phys. Rev. Lett.* 22:679–81
Sodroski TJ. 1991. *Ap. J.* 366:95–106
Sodroski TJ, Odegard N, Dwek E, et al. 1995. *Ap. J.* 452:262
Solomon PM, Edmunds MG, eds. 1980. In *Giant molecular clouds in the galaxy. Proc. Third Gregynog Astrophys. Workshop, Univ. Wales, Cardiff, Wales, Aug. 1977.* Oxford: Pergamon Press
Solomon PM, Klemperer W. 1972. *Ap. J.* 178:389–422
Solomon PM, Rivolo AR. 1989. *Ap. J.* 339:919–25
Solomon PM, Rivolo AR, Barrett J, Yahil A. 1987. *Ap. J.* 319:730–41
Solomon PM, Sanders DB, Scoville NZ. 1979. *Ap. J. Lett.* 232:L89–93
Solomon PM, Wickramasinghe NC. 1969. *Ap. J.* 158:449
Stacy JA, Thaddeus P. 1991. In *Atoms, Ions and Molecules: New Results in Spectral Line Astrophysics*, ed. AD Haschick, PTP Ho. *ASP Conf. Ser.* 16:197–201. San Francisco: ASP
Sternberg A, Dalgarno A. 1995. *Ap. J. Suppl.* 99:565
Sternberg A, Le Petit F, Roueff E, Le Bourlot J. 2014. *Ap. J.* 790:10
Stil JM, Taylor AR, Dickey JM, et al. 2006. *Astron. J.* 132:1158–76
Strong AW, Mattox JR. 1996. *Astron. Astrophys.* 308:L21–24
Stutzki J, Bensch F, Heithausen A, Ossenkopf V, Zielinsky M. 1998. *Astron. Astrophys.* 336:697–720
Stutzki J, Guesten R. 1990. *Ap. J.* 356:513–33

Sunada K, Yamaguchi C, Nakai N, et al. 2000. In *Radio Telescopes*, ed. HR Butcher. *Proc. SPIE Conf. Ser.* 4015:237. Bellingham, WA: SPIE
Swings P, Rosenfeld L. 1937. *Ap. J.* 86:483–86
Tan JC, Krumholz MR, McKee CF. 2006. *Ap. J. Lett.* 641:L121–24
Testi L, Sargent AI. 1998. *Ap. J. Lett.* 508:L91–94
Tielens AGGM, Hollenbach D. 1985. *Ap. J.* 291:722–54
Toomre A. 1964. *Ap. J.* 139:1217–38
Ungerechts H, Umbanhowar P, Thaddeus P. 2000. *Ap. J.* 537:221–35
van der Tak FFS, Black JH, Schöier FL, Jansen DJ, van Dishoeck EF. 2007. *Astron. Astrophys.* 468:627–35
van Dishoeck EF, Black JH. 1988. *Ap. J.* 334:771–802
Vázquez-Semadeni E, Gómez GC, Jappsen AK, et al. 2007. *Ap. J.* 657:870–83
Visser R, van Dishoeck EF, Black JH. 2009. *Astron. Astrophys.* 503:323–43
Vogel SN, Kulkarni SR, Scoville NZ. 1988. *Nature* 334:402–6
Walter F, Brinks E, de Blok WJG, et al. 2008. *Astron. J.* 136:2563–647
Wang QD, Yu KC. 1995. *Astron. J.* 109:698–708
Weinreb S, Barrett AH, Meeks ML, Henry JC. 1963. *Nature* 200:829–31
Williams JP, de Geus EJ, Blitz L. 1994. *Ap. J.* 428:693–712
Williams JP, McKee CF. 1997. *Ap. J.* 476:166
Wilson RW, Jefferts KB, Penzias AA. 1970. *Ap. J. Lett.* 161:L43
Wolfire MG, Hollenbach D, McKee CF. 2010. *Ap. J.* 716:1191–207
Wong T, Hughes A, Ott J, et al. 2011. *Ap. J. Suppl.* 197:16
Wouterloot JGA, Brand J. 1989. *Astron. Astrophys. Suppl.* 80:149–87
Wouterloot JGA, Brand J, Burton WB, Kwee KK. 1990. *Astron. Astrophys.* 230:21–36
Wu YW, Sato M, Reid MJ, et al. 2014. *Astron. Astrophys.* 566:A17
Xu Y, Li JJ, Reid MJ, et al. 2013. *Ap. J.* 769:15
Yamaguchi N, Mizuno N, Saito H, et al. 1999. *Publ. Astron. Soc. Jpn.* 51:775–90
Yoda T, Handa T, Kohno K, et al. 2010. *Publ. Astron. Soc. Jpn.* 62:1277–89
Yonekura Y, Dobashi K, Mizuno A, Ogawa H, Fukui Y. 1997. *Ap. J. Suppl.* 110:21
Zhang B, Reid MJ, Menten KM, et al. 2013. *Ap. J.* 775:79
Zuckerman B, Palmer P. 1974. *Annu. Rev. Astron. Astrophys.* 12:279–313

Annual Review of Astronomy and Astrophysics

Volume 53, 2015

Contents

Indexes

Errata

An online log of corrections to *Annual Review of Astronomy and Astrophysics* articles may be found at http://www.annualreviews.org/errata/astro